Article:
Marin, L, Karageorghis, A and Lesnic, D (2015) A numerical study of the SVDMFS solution of inverse boundary value problems in two-dimensional steady-state linear thermoelasticity. Numerical Methods for Partial Differential Equations, 31 (1). 168 - 201. ISSN 0749-159X

https://doi.org/10.1002/num.21898

A numerical study of the SVD-MFS solution of inverse boundary value problems in two-dimensional steady-state linear thermoelasticity

Liviu Marin[1,2,*], Andreas Karageorghis[3,†], Daniel Lesnic[4,‡]

[1]Department of Mathematics, Faculty of Mathematics and Computer Science, University of Bucharest, 14 Academiei, 010014 Bucharest, Romania
[2]Institute of Solid Mechanics, Romanian Academy, 15 Constantin Mille, 010141 Bucharest, Romania
[3]Department of Mathematics and Statistics, University of Cyprus/Πανεπιστήμιο Κύπρου, P.O. Box 20537, 1678 Nicosia/Λευκωσία, Cyprus/Κύπρος
[4]Department of Applied Mathematics, University of Leeds, Leeds LS2 9JT, UK

Abstract

We study the reconstruction of the missing thermal and mechanical data on an inaccessible part of the boundary in the case of two-dimensional linear isotropic thermoelastic materials from over-prescribed noisy measurements taken on the remaining accessible boundary part. This inverse problem is solved by employing the method of fundamental solutions together with the method of particular solutions. The stabilisation of this inverse problem is achieved by using several singular value decomposition (SVD)-based regularization methods, such as the Tikhonov regularization method [36], the damped SVD and the truncated SVD [37], whilst the optimal regularization parameter is selected according to the discrepancy principle [38], generalized cross-validation criterion [39] and Hansen's L-curve method [40].

Keywords: Linear thermoelasticity; Inverse boundary value problem; Method of fundamental solutions (MFS); Method of particular solutions (MPS); Singular value decomposition (SVD); Regularization.

1 Introduction

For an isotropic material at a uniform reference temperature, a small uniform increase in the temperature field can produce a pure volumetric expansion, provided that the solid body is not constrained against such a movement. This phenomenon can be expressed in terms of the so-called thermal strain, which is related to the difference between the temperature of the solid and the reference temperature through the coefficient of thermal expansion. Such a thermal expansion may also occur with no stresses present in the solid body [1]. Consequently, whenever a solid is subject to heating conditions that give rise to a temperature distribution throughout its volume, it is important to perform the stress analysis of the solid body by assuming it to be subject to thermal and mechanical loadings, i.e. thermoelastic loadings.

The mathematical problems associated with isotropic thermoelastic solids have been the subject of numerous studies using various numerical methods such as the boundary element method (BEM) [2–6], the dual reciprocity BEM (DRBEM) [7], the finite element method (FEM) [8, 9], the moving least-squares method combined with the local boundary integral method [10], the method of fundamental solutions (MFS) [11–13], etc. In the case of direct problems in thermoelasticity, the thermo-mechanical equilibrium equations have to be solved in a known geometry subject to known material constants,

*Corresponding author. E-mails: marin.liviu@gmail.com; liviu.marin@fmi.unibuc.ro
†E-mail: andreask@ucy.ac.cy
‡E-mail: amt5ld@maths.leeds.ac.uk

prescribed heat sources and/or body forces, and appropriate initial and boundary conditions for the temperature, normal heat flux, displacement and traction vectors. The total or partial lack of knowledge of at least one of these conditions leads to a so-called *inverse problem*. A classical example of an inverse problem is represented by *inverse boundary value problems* in which the geometry of the solution domain, the thermo-mechanical material constants and the heat sources and body forces are all known, while boundary data are not available on an inaccessible part of the boundary and instead over-prescribed boundary conditions are provided on the remaining boundary part. It is well-known that inverse boundary value problems are generally ill-posed [14], in the sense that the existence, uniqueness and stability of their solutions are not always guaranteed. For these reasons, particular care is required in the numerical solution of such problems.

The MFS is a meshless boundary collocation method which belongs to the family of so-called Trefftz methods [15, 16] and is applicable to boundary value problems for which a fundamental solution of the operator in the governing equation is known. Despite this restriction, the MFS has become very popular primarily because of the ease with which it can be implemented, in particular for the solution of problems in complex geometries. Since its introduction as a numerical method [17], it has been successfully applied to a large variety of physical problems, an account of which may be found in the survey papers by Fairweather and Karageorghis [18], Fairweather et al. [19], Golberg and Chen [20], and Karageorghis et al. [21].

Furthermore, the MFS in conjunction with various regularization methods such as the Tikhonov regularization method (TRM) and singular value decomposition (SVD), has been used increasingly over the last decade for the numerical solution of inverse problems. For example, the Cauchy problem associated with the heat conduction equation [22–25], linear elasticity [26, 27], steady-state heat conduction in functionally graded materials [28], Helmholtz-type equations [25, 29–31], Stokes problems [32], the biharmonic equation [33], etc. have all been successfully solved by the MFS. For a survey of applications of the MFS to inverse problems, we refer the reader to Karageorghis et al. [21].

Both the Cauchy problem and the general inverse boundary value problem in static planar thermoelasticity have recently been addressed by Marin and Karageorghis [34], and Karageorghis et al. [35], respectively, who applied the MFS, Hansen's L-curve criterion and the numerical inversion of the normal system of equations generated by the minimisation of the zeroth-order Tikhonov functional. In this paper, we investigate these problems again more thoroughly by employing a wider range of SVD-based non-iterative regularization methods, such as TRM [36], the damped SVD (DSVD) and the truncated SVD (TSVD) [37]. Furthermore, we investigate several criteria for the selection of the regularization parameter which can be chosen according to Morozov's discrepancy principle (DP) [38], generalized cross-validation (GCV) criterion [39] and Hansen's L-curve (LC) method [40]. Also, a comparison of the numerical results retrieved for every possible coupling regularization method-selection criterion is made.

The paper is organised as follows: In Section 2 we formulate mathematically the inverse problems under investigation. The proposed algorithm is described in Section 3, while the MFS-MPS approach is presented in Section 4. The aforementioned SVD-based regularization methods, as well as the criteria for the selection of the optimal regularization parameter, are briefly presented in Section 5. The accuracy and stability of the numerical results obtained using these regularization methods and selection criteria are thoroughly analysed for three examples in Section 6. Finally, some conclusions are presented in Section 7.

2 Mathematical Formulation

We consider an isotropic solid which occupies a bounded planar domain $\Omega \subset \mathbb{R}^2$, and is characterised by the following material constants: the thermal conductivity, κ, the coefficient of linear thermal expansion, α_{T}, Poisson's ratio, ν, and the shear modulus, G.

In the framework of isotropic linear thermoelasticity, the strain tensor, $\boldsymbol{\epsilon} = [\epsilon_{ij}]_{1\leq i,j\leq 2}$, satisfies the

kinematic relation

$$\boldsymbol{\epsilon}(\mathbf{x}) = \frac{1}{2}\left(\nabla\mathbf{u}(\mathbf{x}) + \nabla\mathbf{u}(\mathbf{x})^{\mathsf{T}}\right), \quad \mathbf{x} \in \overline{\Omega}\,, \tag{1}$$

and is related to the stress tensor, $\boldsymbol{\sigma} = [\sigma_{ij}]_{1\le i,j\le 2}$, by means of the following constitutive law [1]

$$\boldsymbol{\sigma}(\mathbf{x}) = 2G\left[\boldsymbol{\epsilon}(\mathbf{x}) + \frac{\overline{\nu}}{1-2\overline{\nu}}\,\mathrm{tr}\,(\boldsymbol{\epsilon}(\mathbf{x}))\,\mathbf{I}\right] - \overline{\gamma}\,\mathrm{T}(\mathbf{x})\,\mathbf{I}\,, \quad \mathbf{x} \in \overline{\Omega}. \tag{2}$$

Here $\mathbf{I} = [\delta_{ij}]_{1\le i,j\le 2}$, $\overline{\nu}$ is the equivalent Poisson's ratio ($\overline{\nu} = \nu$ for a plane strain state and $\overline{\nu} = \nu/(1+\nu)$ for a plane stress state), while the constant $\overline{\gamma}$ is given by

$$\overline{\gamma} = 2G\,\overline{\alpha}_{\mathrm{T}}(1+\overline{\nu})/(1-2\overline{\nu})\,, \tag{3}$$

where $\overline{\alpha}_{\mathrm{T}}$ is the equivalent coefficient of linear expansion $\big(\overline{\alpha}_{\mathrm{T}} = \alpha_{\mathrm{T}}$ and $\overline{\alpha}_{\mathrm{T}} = \alpha_{\mathrm{T}}\,(1+\nu)/(1+2\nu)$ for the plane strain and plane stress states, respectively$\big)$. The kinematic relation (1) combined with the constitutive law of isotropic thermoelasticity (2) yields

$$\boldsymbol{\sigma}(\mathbf{x}) = G\left[\left(\nabla\mathbf{u}(\mathbf{x}) + \nabla\mathbf{u}(\mathbf{x})^{\mathsf{T}}\right) + \frac{2\overline{\nu}}{1-2\overline{\nu}}\big(\nabla\cdot\mathbf{u}(\mathbf{x})\big)\mathbf{I}\right] - \overline{\gamma}\,\mathrm{T}(\mathbf{x})\,\mathbf{I}\,, \quad \mathbf{x} \in \overline{\Omega}\,. \tag{4}$$

In the absence of body forces, the equilibrium equations of two-dimensional isotropic linear thermoelasticity, in terms of the displacement vector and the temperature, become

$$-\nabla\cdot\boldsymbol{\sigma}(\mathbf{x}) \equiv \mathscr{L}\mathbf{u}(\mathbf{x}) + \overline{\gamma}\,\nabla\mathrm{T}(\mathbf{x}) = \mathbf{0}\,, \quad \mathbf{x} \in \Omega\,, \tag{5}$$

where $\mathscr{L} = (\mathscr{L}_1, \mathscr{L}_2)^{\mathsf{T}}$ is the partial differential operator associated with the Navier-Lamé system of isotropic linear elasticity, i.e.

$$\mathscr{L}\mathbf{u}(\mathbf{x}) \equiv -G\left[\nabla\cdot\left(\nabla\mathbf{u}(\mathbf{x}) + \nabla\mathbf{u}(\mathbf{x})^{\mathsf{T}}\right) + \frac{2\overline{\nu}}{1-2\overline{\nu}}\nabla\big(\nabla\cdot\mathbf{u}(\mathbf{x})\big)\right], \ \mathbf{x} \in \Omega\,. \tag{6}$$

In the absence of heat sources, the governing steady-state heat conduction equation becomes

$$-\nabla\cdot\big(\kappa\,\nabla\mathrm{T}(\mathbf{x})\big) = 0\,, \quad \mathbf{x} \in \Omega\,. \tag{7}$$

Further, we let $\mathbf{n}(\mathbf{x})$ be the outward unit normal vector to the boundary $\partial\Omega$ of Ω, $\mathrm{q}(\mathbf{x})$ be the normal heat flux at a point $\mathbf{x} \in \partial\Omega$ defined by

$$\mathrm{q}(\mathbf{x}) \equiv -\big(\kappa\,\nabla\mathrm{T}(\mathbf{x})\big)\cdot\mathbf{n}(\mathbf{x}), \quad \mathbf{x} \in \partial\Omega, \tag{8}$$

and $\mathbf{t}(\mathbf{x})$ be the traction vector at $\mathbf{x} \in \partial\Omega$ given by

$$\mathbf{t}(\mathbf{x}) \equiv \boldsymbol{\sigma}(\mathbf{x})\,\mathbf{n}(\mathbf{x}), \quad \mathbf{x} \in \partial\Omega. \tag{9}$$

In the direct (forward) formulation, the temperature and normal heat flux are prescribed on the boundaries Γ_{T} and Γ_{q}, respectively, where $\Gamma_{\mathrm{T}} \cup \Gamma_{\mathrm{q}} = \partial\Omega$ and $\Gamma_{\mathrm{T}} \cap \Gamma_{\mathrm{q}} = \varnothing$, while the displacement and traction vectors are given on the boundaries $\Gamma_{\mathbf{u}}$ and $\Gamma_{\mathbf{t}}$, respectively, where $\Gamma_{\mathbf{u}} \cup \Gamma_{\mathbf{t}} = \partial\Omega$ and $\Gamma_{\mathbf{u}} \cap \Gamma_{\mathbf{t}} = \varnothing$. However, in many practical situations, only a part of the boundary, say $\Gamma_1 \subset \partial\Omega$, is accessible for measurements, while the remaining boundary part, $\Gamma_2 = \partial\Omega \setminus \overline{\Gamma}_1$, is inaccessible and hence no boundary data is available on it. In such a situation, additional measurements are available on Γ_1, hence compensating for the lack of boundary data on Γ_2, and this corresponds to an inverse boundary value problem.

In the sequel, we consider the following two inverse boundary value problems for two-dimensional steady-state isotropic linear thermoelasticity:

Problem (A): The *Cauchy problem* given by the partial differential equations (5) and (7) and the following over-prescribed thermal and mechanical boundary conditions:

$$\mathrm{T}(\mathbf{x}) = \widetilde{\mathrm{T}}(\mathbf{x}) \quad \text{and} \quad \mathrm{q}(\mathbf{x}) = \widetilde{\mathrm{q}}(\mathbf{x}), \quad \mathbf{x} \in \Gamma_1, \tag{10a}$$

$$\mathbf{u}(\mathbf{x}) = \widetilde{\mathbf{u}}(\mathbf{x}) \quad \text{and} \quad \mathbf{t}(\mathbf{x}) = \widetilde{\mathbf{t}}(\mathbf{x}), \quad \mathbf{x} \in \Gamma_1. \tag{10b}$$

Problem (B): The *inverse boundary value problem* consisting of the partial differential equations (5) and (7) and the following boundary conditions:

$$\mathrm{T}(\mathbf{x}) = \widetilde{\mathrm{T}}(\mathbf{x}), \quad \mathbf{x} \in \Gamma_1, \tag{11a}$$

$$\mathbf{u}(\mathbf{x}) = \widetilde{\mathbf{u}}(\mathbf{x}), \quad \mathbf{x} \in \Gamma_1, \tag{11b}$$

$$\mathbf{t}(\mathbf{x}) = \widetilde{\mathbf{t}}(\mathbf{x}), \quad \mathbf{x} \in \partial\Omega. \tag{11c}$$

In equations (10) and (11), $\widetilde{\mathrm{T}}$, $\widetilde{\mathrm{q}}$, $\widetilde{\mathbf{u}}$ and $\widetilde{\mathbf{t}}$ are prescribed boundary temperature, normal heat flux, displacements and tractions, respectively. Each of the inverse problems consisting of the governing equations (5) and (7), together with the boundary conditions (10a)–(10b) or (11a)–(11c), is considerably more difficult to solve both analytically and numerically than direct problems since its solution does not satisfy the general conditions of well-posedness [14]. Consequently, direct methods, such as the least-squares method, will fail to produce stable and physically meaningful solutions to these problems and hence suitable regularization procedures should be employed.

3 Solution Algorithm

The main idea of the present approach relies on employing a particular solution of the inhomogeneous equilibrium equations (5) according to the method developed by Marin and Karageorghis [12, 34]. By using the linearity of the governing partial differential operators involved in equations (5) and (7), we transform the original inverse problem (A) or (B) into a corresponding homogeneous inverse problem via the superposition principle. The resulting discretised inverse problem is solved, in a stable manner, by employing a regularization method based on the SVD, namely the TRM [36], the DSVD or the TSVD [37].

The procedure described above may be summarised, e.g. for the inverse boundary value problem (B), as follows:

Step 1. Determine a particular solution $\big(\mathrm{T}^{(\mathsf{P})}, \mathbf{u}^{(\mathsf{P})}\big)$ in $\widetilde{\Omega} \supset \Omega$ of the heat equation (7) and the non-homogeneous equilibrium equations (5), respectively,

$$-\nabla \cdot \big(\kappa\, \nabla \mathrm{T}^{(\mathsf{P})}(\mathbf{x})\big) = 0\,, \quad \mathbf{x} \in \widetilde{\Omega} \supset \Omega, \tag{12a}$$

$$\mathscr{L}\mathbf{u}^{(\mathsf{P})}(\mathbf{x}) + \overline{\gamma}\, \nabla \mathrm{T}^{(\mathsf{P})}(\mathbf{x}) = \mathbf{0}\,, \quad \mathbf{x} \in \widetilde{\Omega} \supset \Omega, \tag{12b}$$

as well as the corresponding particular normal heat flux

$$\mathrm{q}^{(\mathsf{P})}(\mathbf{x}) = -\big(\kappa\, \nabla \mathrm{T}^{(\mathsf{P})}(\mathbf{x})\big) \cdot \mathbf{n}(\mathbf{x}), \quad \mathbf{x} \in \partial\Omega, \tag{12c}$$

strain tensor

$$\boldsymbol{\epsilon}^{(\mathsf{P})}(\mathbf{x}) = \frac{1}{2}\left(\nabla \mathbf{u}^{(\mathsf{P})}(\mathbf{x}) + \nabla \mathbf{u}^{(\mathsf{P})}(\mathbf{x})^{\mathsf{T}}\right), \quad \mathbf{x} \in \overline{\Omega}\,, \tag{12d}$$

stress tensor

$$\boldsymbol{\sigma}^{(\mathsf{P})}(\mathbf{x}) = 2G\left[\boldsymbol{\epsilon}^{(\mathsf{P})}(\mathbf{x}) + \frac{\overline{\nu}}{1-2\overline{\nu}}\, \mathrm{tr}\big(\boldsymbol{\epsilon}^{(\mathsf{P})}(\mathbf{x})\big)\, \mathbf{I}\right], \quad \mathbf{x} \in \overline{\Omega}\,, \tag{12e}$$

and traction vector

$$\mathbf{t}^{(\mathsf{P})}(\mathbf{x}) = \boldsymbol{\sigma}^{(\mathsf{P})}(\mathbf{x})\, \mathbf{n}(\mathbf{x})\,, \quad \mathbf{x} \in \partial\Omega\,. \tag{12f}$$

Step 2. Solve the resulting inverse boundary value problem associated with the homogeneous thermal and mechanical equilibrium equations, i.e.

$$-\nabla \cdot \left(\kappa \, \nabla \mathrm{T}^{(\mathsf{H})}(\mathbf{x})\right) = 0, \quad \mathbf{x} \in \Omega, \tag{13a}$$

$$\mathscr{L}\mathbf{u}^{(\mathsf{H})}(\mathbf{x}) = \mathbf{0}, \quad \mathbf{x} \in \Omega, \tag{13b}$$

$$\mathrm{T}^{(\mathsf{H})}(\mathbf{x}) = \widetilde{\mathrm{T}}(\mathbf{x}) - \mathrm{T}^{(\mathsf{P})}(\mathbf{x}), \quad \mathbf{x} \in \Gamma_1, \tag{13c}$$

$$\mathbf{u}^{(\mathsf{H})}(\mathbf{x}) = \widetilde{\mathbf{u}}(\mathbf{x}) - \mathbf{u}^{(\mathsf{P})}(\mathbf{x}), \quad \mathbf{x} \in \Gamma_1, \tag{13d}$$

$$\mathbf{t}^{(\mathsf{H})}(\mathbf{x}) - \overline{\gamma}\,\mathrm{T}^{(\mathsf{H})}(\mathbf{x})\,\mathbf{n}(\mathbf{x}) = \widetilde{\mathbf{t}}(\mathbf{x}) - \left[\mathbf{t}^{(\mathsf{P})}(\mathbf{x}) - \overline{\gamma}\,\mathrm{T}^{(\mathsf{P})}(\mathbf{x})\,\mathbf{n}(\mathbf{x})\right], \quad \mathbf{x} \in \partial\Omega, \tag{13e}$$

using one of the SVD-based regularization methods mentioned above to determine $\mathrm{T}^{(\mathsf{H})}\big|_{\Omega\cup\Gamma_2}$, $\mathrm{q}^{(\mathsf{H})}\big|_{\partial\Omega}$ and $\mathbf{u}^{(\mathsf{H})}\big|_{\Omega\cup\Gamma_2}$.

Step 3. Apply the superposition principle to determine the unknown thermo-mechanical fields, namely $\mathrm{T}\big|_{\Omega\cup\Gamma_2} = \mathrm{T}^{(\mathsf{P})}\big|_{\Omega\cup\Gamma_2} + \mathrm{T}^{(\mathsf{H})}\big|_{\Omega\cup\Gamma_2}$, $\mathrm{q}\big|_{\partial\Omega} = \mathrm{q}^{(\mathsf{P})}\big|_{\partial\Omega} + \mathrm{q}^{(\mathsf{H})}\big|_{\partial\Omega}$, $\mathbf{u}\big|_{\Omega\cup\Gamma_2} = \mathbf{u}^{(\mathsf{P})}\big|_{\Omega\cup\Gamma_2} + \mathbf{u}^{(\mathsf{H})}\big|_{\Omega\cup\Gamma_2}$, $\boldsymbol{\epsilon}\big|_{\Omega} = \boldsymbol{\epsilon}^{(\mathsf{P})}\big|_{\Omega} + \boldsymbol{\epsilon}^{(\mathsf{H})}\big|_{\Omega}$ and $\boldsymbol{\sigma}\big|_{\Omega} = \boldsymbol{\sigma}^{(\mathsf{P})}\big|_{\Omega} + \boldsymbol{\sigma}^{(\mathsf{H})}\big|_{\Omega} - \overline{\gamma}\,\mathrm{T}\big|_{\Omega}\,\mathbf{I}$.

The proposed algorithm relies on the existence of a particular solution of the homogeneous heat equation (7) and the non-homogeneous equilibrium equations (5) which is justified by the following result, see e.g. Marin and Karageorghis [12] for further details:

Proposition 1. *Let $\Omega \subset \mathbb{R}^2$ be a bounded planar domain occupied by an isotropic thermoelastic solid characterised by the constant thermal conductivity, κ, the coefficient of linear thermal expansion, α_{T}, Poisson's ratio, ν, and the shear modulus, G, and let $\overline{\gamma}$ be given by equation* (3).

Then, for any set $\mathbb{X}_K = \left\{\mathbf{x}^{(k)}\right\}_{k=\overline{1,K}} \subset \mathbb{R}^2 \setminus \overline{\Omega}$, $K \in \mathbb{Z}_+$, the temperature field

$$\mathrm{T}^{(\mathsf{P})}(\mathbf{x}) = \sum_{k=1}^{K} \mathrm{T}_k \, \log\|\mathbf{x} - \mathbf{x}^{(k)}\|, \quad \mathbf{x} \in \overline{\Omega}, \tag{14a}$$

where $\mathrm{T}_k \in \mathbb{R}$, $k = \overline{1,K}$, and the displacement vector

$$\mathbf{u}^{(\mathsf{P})}(\mathbf{x}) = \frac{\mathrm{c}^{(\mathsf{P})}}{2G} \sum_{k=1}^{K} \mathrm{T}_k \left(\mathbf{x} - \mathbf{x}^{(k)}\right) \log\|\mathbf{x} - \mathbf{x}^{(k)}\|, \quad \mathbf{x} \in \overline{\Omega}, \tag{14b}$$

where

$$\mathrm{c}^{(\mathsf{P})} := \frac{\overline{\gamma}}{2}\left(\frac{1-2\overline{\nu}}{1-\overline{\nu}}\right) = G\overline{\alpha}_{\mathrm{T}}\left(\frac{1+\overline{\nu}}{1-\overline{\nu}}\right), \tag{14c}$$

represent a particular solution $\left(\mathrm{T}^{(\mathsf{P})}, \mathbf{u}^{(\mathsf{P})}\right) \in \mathrm{C}^{\infty}\left(\overline{\Omega}\right) \times \left(\mathrm{C}^{\infty}\left(\overline{\Omega}\right)\right)^2$ of the governing equations (5) *and* (7) *of two-dimensional isotropic linear thermoelasticity.*

As a direct consequence of Proposition 1, the expressions for the corresponding particular strain tensor, $\boldsymbol{\epsilon}^{(\mathsf{P})}$, stress tensor $\boldsymbol{\sigma}^{(\mathsf{P})}$, and traction vector $\mathbf{t}^{(\mathsf{P})}$, are obtained by substituting the particular displacement vector given by (14b) into equations (12d)–(12f), respectively, i.e.

$$\boldsymbol{\epsilon}^{(\mathsf{P})}(\mathbf{x}) = \frac{\mathrm{c}^{(\mathsf{P})}}{2G} \sum_{k=1}^{K} \mathrm{T}_k \left[\log\|\mathbf{x} - \mathbf{x}^{(k)}\|\,\mathbf{I} + \frac{\mathbf{x} - \mathbf{x}^{(k)}}{\|\mathbf{x} - \mathbf{x}^{(k)}\|} \otimes \frac{\mathbf{x} - \mathbf{x}^{(k)}}{\|\mathbf{x} - \mathbf{x}^{(k)}\|}\right], \quad \mathbf{x} \in \overline{\Omega}, \tag{15a}$$

$$\boldsymbol{\sigma}^{(\mathsf{P})}(\mathbf{x}) = \mathrm{c}^{(\mathsf{P})} \sum_{k=1}^{K} \mathrm{T}_k \left[\frac{1}{1-2\overline{\nu}}\left(\log\|\mathbf{x} - \mathbf{x}^{(k)}\| + \overline{\nu}\right)\mathbf{I} + \frac{\mathbf{x} - \mathbf{x}^{(k)}}{\|\mathbf{x} - \mathbf{x}^{(k)}\|} \otimes \frac{\mathbf{x} - \mathbf{x}^{(k)}}{\|\mathbf{x} - \mathbf{x}^{(k)}\|}\right], \quad \mathbf{x} \in \overline{\Omega}, \tag{15b}$$

$$\mathbf{t}^{(\mathsf{P})}(\mathbf{x}) = \mathrm{c}^{(\mathsf{P})} \sum_{k=1}^{K} \mathrm{T}_k \left[\frac{1}{1-2\overline{\nu}} \left(\log \|\mathbf{x}-\mathbf{x}^{(k)}\| + \overline{\nu} \right) \mathbf{n}(\mathbf{x}) + \frac{\left(\mathbf{x}-\mathbf{x}^{(k)}\right)\cdot \mathbf{n}(\mathbf{x})}{\|\mathbf{x}-\mathbf{x}^{(k)}\|^2} \left(\mathbf{x}-\mathbf{x}^{(k)}\right) \right], \quad \mathbf{x} \in \partial\Omega\,. \tag{15c}$$

As will be shown in the next section, the particular solution $\mathbf{u}^{(\mathsf{P})}$ given by equation (14b) is related to the fundamental solution of the two-dimensional Laplace equation (7) through the logarithmic term in (14a) and, consequently, the same remark holds for $\boldsymbol{\epsilon}^{(\mathsf{P})}$, $\boldsymbol{\sigma}^{(\mathsf{P})}$ and $\mathbf{t}^{(\mathsf{P})}$. This remark actually represents the rationale for employing the MFS in conjunction with a suitable regularization method to solve the inverse problems under investigation.

The proposed algorithm can be implemented using any other numerical method which is suitable for discretising the equations (5) and (7) such as the BEM, the FEM, or the finite-difference method (FDM), together with the particular solution given by Proposition 1.

4 Method of Fundamental Solutions

4.1 MFS Approximation for the Thermal Problem

The fundamental solution of the two-dimensional steady-state heat conduction in an isotropic homogeneous (κ = constant) medium, i.e. the Laplace equation, is given by

$$\mathsf{F}(\mathbf{x},\boldsymbol{\xi}) = -\frac{1}{2\pi\kappa} \log\|\mathbf{x}-\boldsymbol{\xi}\|, \quad \mathbf{x} \in \overline{\Omega}, \tag{16}$$

where $\boldsymbol{\xi} = (\xi_1, \xi_2) \in \mathbb{R}^2 \backslash \overline{\Omega}$ is a source or singularity point. In the MFS, the temperature is approximated by a linear combination of fundamental solutions with respect to N_L sources, $\left\{\boldsymbol{\xi}^{(n)}\right\}_{n=\overline{1,N_L}}$, in the form

$$\mathrm{T}(\mathbf{x}) \approx \mathrm{T}_{N_L}(\mathbf{c}^{(1)}, \boldsymbol{\xi}; \mathbf{x}) = \sum_{n=1}^{N_L} \mathsf{F}\left(\mathbf{x}, \boldsymbol{\xi}^{(n)}\right) \mathrm{c}_n^{(1)}\,, \quad \mathbf{x} \in \overline{\Omega}\,, \tag{17}$$

where $\mathbf{c}^{(1)} = \left(\mathrm{c}_1^{(1)}, \ldots, \mathrm{c}_{N_L}^{(1)}\right) \in \mathbb{R}^{N_L}$ and $\boldsymbol{\xi} \in \mathbb{R}^{2N_L}$ is a vector containing the coordinates of the sources. We observe that if one takes $\mathrm{T}_n := -\mathrm{c}_n^{(1)} / (2\pi\kappa)$, $n = \overline{1, N_L}$, in equation (17), then the latter represents the expression of a particular solution, as given by relation (14a) with $\mathbb{X}_{N_L} = \left\{\boldsymbol{\xi}^{(n)}\right\}_{n=\overline{1,N_L}} \subset \mathbb{R}^2 \setminus \overline{\Omega}$, i.e. $\mathrm{T}(\mathbf{x}) \approx \mathrm{T}^{(\mathsf{P})}(\mathbf{x})$ for $\mathbf{x} \in \overline{\Omega}$ or, equivalently, $\mathrm{T}(\mathbf{x}) = \mathrm{T}^{(\mathsf{P})}(\mathbf{x}) + \mathrm{T}^{(\mathsf{H})}(\mathbf{x})$ for $\mathbf{x} \in \overline{\Omega}$, with $\mathrm{T}^{(\mathsf{H})}(\mathbf{x}) \approx 0$, $\mathbf{x} \in \overline{\Omega}$.

From equations (8) and (16), it follows that the normal heat flux can be approximated by

$$\mathrm{q}(\mathbf{x}) \approx \mathrm{q}_{N_L}(\mathbf{c}^{(1)}, \boldsymbol{\xi}; \mathbf{x}) = -\sum_{n=1}^{N_L} \left[\kappa \nabla_{\mathbf{x}} \mathsf{F}\left(\mathbf{x}, \boldsymbol{\xi}^{(n)}\right) \cdot \mathbf{n}(\mathbf{x}) \right] \mathrm{c}_n^{(1)}, \quad \mathbf{x} \in \partial\Omega\,. \tag{18}$$

We mention that, analogous to equation (17), expression (18) actually means that $\mathrm{q}(\mathbf{x}) \approx \mathrm{q}^{(\mathsf{P})}(\mathbf{x})$ for $\mathbf{x} \in \partial\Omega$ or, equivalently, $\mathrm{q}(\mathbf{x}) = \mathrm{q}^{(\mathsf{P})}(\mathbf{x}) + \mathrm{q}^{(\mathsf{H})}(\mathbf{x})$ for $\mathbf{x} \in \overline{\Omega}$, with $\mathrm{q}^{(\mathsf{H})}(\mathbf{x}) \approx 0$, $\mathbf{x} \in \partial\Omega$.

Next, we select M_L^1 collocation points, $\left\{\mathbf{x}^{(n)}\right\}_{n=\overline{1,M_L^1}}$, on the boundary Γ_1 and M_L^2 collocation points, $\left\{\mathbf{x}^{(M_L^1+n)}\right\}_{n=\overline{1,M_L^2}}$, on the boundary Γ_2, such that $M_L^1 + M_L^2 = M_L$. By collocating the thermal boundary conditions (10a) or (11a), one obtains the following linear system of equations for the unknown coefficients $\mathbf{c}^{(1)} \in \mathbb{R}^{N_L}$:

$$\mathbf{A}^{(11)}\, \mathbf{c}^{(1)} = \mathbf{f}^{(1)}. \tag{19}$$

Here $\mathbf{A}^{(11)} \in \mathbb{R}^{dM_L^1 \times N_L}$ is the MFS matrix associated with the thermal part of the inverse problem under investigation and $\mathbf{f}^{(1)} \in \mathbb{R}^{dM_L^1}$ contains the corresponding discretised thermal data available on Γ_1, where $d = 2$ for the Cauchy problem (A), and $d = 1$ in the case of the inverse boundary value problem (B).

4.2 MFS Approximation for the Non-Homogeneous Equilibrium Equations

The MFS approximation for the particular solution to the non-homogeneous equilibrium equations (5) in $\mathbb{R}^2$ is given by [12]

$$\mathbf{u}^{(\mathsf{P})}(\mathbf{y}) \approx \mathbf{u}^{(\mathsf{P})}_{N_L}(\mathbf{c}^{(1)}, \boldsymbol{\xi}; \mathbf{y}) = \frac{\mathrm{c}^{(\mathsf{P})}}{2G} \sum_{n=1}^{N_L} \mathsf{F}\big(\mathbf{y}, \boldsymbol{\xi}^{(n)}\big) \, \big(\mathbf{y} - \boldsymbol{\xi}^{(n)}\big) \, \mathrm{c}^{(1)}_n \,, \quad \mathbf{y} \in \mathbb{R}^2 \setminus \mathbb{X}_{N_L}. \tag{20}$$

The corresponding approximation for the particular traction vector is obtained as

$$\begin{aligned} \mathbf{t}^{(\mathsf{P})}(\mathbf{y}) \approx \mathbf{t}^{(\mathsf{P})}_{N_L}(\mathbf{c}^{(1)}, \boldsymbol{\xi}; \mathbf{y}) = -\mathrm{c}^{(\mathsf{P})} \sum_{n=1}^{N_L} \Bigg[\bigg(\frac{1}{1-2\overline{\nu}} \, \mathsf{F}\big(\mathbf{y}, \boldsymbol{\xi}^{(n)}\big) + \frac{1}{2\pi\kappa} \, \frac{\overline{\nu}}{1-2\overline{\nu}} \bigg) \, \mathbf{n}(\mathbf{y}) \\ + \frac{1}{2\pi\kappa} \left(\frac{\mathbf{y} - \boldsymbol{\xi}^{(n)}}{\|\mathbf{y} - \boldsymbol{\xi}^{(n)}\|} \cdot \mathbf{n}(\mathbf{y}) \right) \frac{\mathbf{y} - \boldsymbol{\xi}^{(n)}}{\|\mathbf{y} - \boldsymbol{\xi}^{(n)}\|} \Bigg] \mathrm{c}^{(1)}_n \,, \quad \mathbf{y} \in \partial\Omega \,. \end{aligned} \tag{21}$$

Consequently, the term $\big(\mathbf{t}^{(\mathsf{P})} - \overline{\gamma}\, \mathrm{T}^{(\mathsf{P})}\, \mathbf{n}\big)\big|_{\partial\Omega}$, which is needed in (13e), is approximated by

$$\begin{aligned} &\big(\mathbf{t}^{(\mathsf{P})}(\mathbf{y}) - \overline{\gamma}\, \mathrm{T}^{(\mathsf{P})}(\mathbf{y})\, \mathbf{n}(\mathbf{y})\big)\big|_{\mathbf{y}\in\partial\Omega} \approx \Big(\mathbf{t}^{(\mathsf{P})}_{N_L}(\mathbf{c}^{(1)}, \boldsymbol{\xi}; \mathbf{y}) - \overline{\gamma}\, \mathrm{T}_{N_L}(\mathbf{y})\, \mathbf{n}(\mathbf{y})\Big)\big|_{\mathbf{y}\in\partial\Omega} \\ &= -\mathrm{c}^{(\mathsf{P})} \sum_{n=1}^{N_L} \Bigg[\bigg(-\mathsf{F}\big(\mathbf{y}, \boldsymbol{\xi}^{(n)}\big) + \frac{1}{2\pi\kappa} \, \frac{\overline{\nu}}{1-2\overline{\nu}} \bigg) \, \mathbf{n}(\mathbf{y}) + \frac{1}{2\pi\kappa} \left(\frac{\mathbf{y} - \boldsymbol{\xi}^{(n)}}{\|\mathbf{y} - \boldsymbol{\xi}^{(n)}\|} \cdot \mathbf{n}(\mathbf{y}) \right) \frac{\mathbf{y} - \boldsymbol{\xi}^{(n)}}{\|\mathbf{y} - \boldsymbol{\xi}^{(n)}\|} \Bigg] \mathrm{c}^{(1)}_n \,. \end{aligned} \tag{22}$$

4.3 MFS Approximation for the Homogeneous Mechanical Problem

As a direct consequence of the MFS approximation for the thermal problem, the second step of the proposed algorithm (13a)–(13e) reduces to equations (13b), (13d) and (13e) with $\mathrm{T}^{(\mathsf{H})}(\mathbf{x}) \approx 0$ for $\mathbf{x} \in \partial\Omega$ and these actually represent the equilibrium equations of two-dimensional isotropic linear elasticity in the absence of body forces for $\mathbf{u}^{(\mathsf{H})}$ in Ω with over-specified boundary conditions.

The fundamental solution matrix $\mathbf{U} = [\mathsf{U}_{ij}]_{1\le i,j\le 2}$, for the displacement vector in the Cauchy-Navier system is given by [41]

$$\mathsf{U}_{ij}(\mathbf{y}, \boldsymbol{\eta}) = \frac{1}{8\pi G(1-\overline{\nu})} \left[-(3-4\overline{\nu}) \, \log\|\mathbf{y} - \boldsymbol{\eta}\| \, \delta_{ij} + \frac{\mathrm{y}_i - \eta_i}{\|\mathbf{x} - \boldsymbol{\eta}\|} \, \frac{\mathrm{y}_j - \eta_j}{\|\mathbf{x} - \boldsymbol{\eta}\|} \right], \quad \mathbf{y} \in \overline{\Omega} \,, \quad i, j = 1, 2 \,, \tag{23}$$

where $\mathbf{y} = (\mathrm{y}_1, \mathrm{y}_2) \in \overline{\Omega}$ is a collocation point and $\boldsymbol{\eta} = (\eta_1, \eta_2) \in \mathbb{R}^2 \setminus \overline{\Omega}$ is a source point.

By differentiating equation (23) with respect to y_k, $k = 1, 2$, one obtains the derivatives of the fundamental solution for the displacement vector, denoted by $\partial_{\mathrm{y}_k} \mathsf{U}_{ij}(\mathbf{y}, \boldsymbol{\eta})$, where $\partial_{\mathrm{y}_k} \equiv \partial / \partial \mathrm{y}_k$. The fundamental solution matrix $\mathbf{T} = [\mathsf{T}_{ij}]_{1\le i,j\le 2}$, for the traction vector in the case of two-dimensional isotropic linear elasticity is then obtained by combining equation (23) with the definition of the traction vector and Hooke's constitutive law of isotropic linear elasticity [41], namely

$$\begin{aligned} \mathsf{T}_{1k}(\mathbf{y}, \boldsymbol{\eta}) = \frac{2G}{1-2\overline{\nu}} \Big[(1-\overline{\nu}) \, \partial_{\mathrm{y}_1} \mathsf{U}_{1k}(\mathbf{y}, \boldsymbol{\eta}) + \overline{\nu} \, \partial_{\mathrm{y}_2} \mathsf{U}_{2k}(\mathbf{y}, \boldsymbol{\eta}) \Big] \, \mathrm{n}_1(\mathbf{y}) \\ + G \Big[\partial_{\mathrm{y}_2} \mathsf{U}_{1k}(\mathbf{y}, \boldsymbol{\eta}) + \partial_{\mathrm{y}_1} \mathsf{U}_{2k}(\mathbf{y}, \boldsymbol{\eta}) \Big] \, \mathrm{n}_2(\mathbf{y}), \quad \mathbf{y} \in \partial\Omega \,, \quad k = 1, 2, \end{aligned} \tag{24a}$$

and

$$\begin{aligned} \mathsf{T}_{2k}(\mathbf{y}, \boldsymbol{\eta}) = G \Big[\partial_{\mathrm{y}_2} \mathsf{U}_{1k}(\mathbf{y}, \boldsymbol{\eta}) + \partial_{\mathrm{y}_1} \mathsf{U}_{2k}(\mathbf{y}, \boldsymbol{\eta}) \Big] \, \mathrm{n}_1(\mathbf{y}) \\ + \frac{2G}{1-2\overline{\nu}} \Big[\overline{\nu} \, \partial_{\mathrm{y}_1} \mathsf{U}_{1k}(\mathbf{y}, \boldsymbol{\eta}) + (1-\overline{\nu}) \, \partial_{\mathrm{y}_2} \mathsf{U}_{2k}(\mathbf{y}, \boldsymbol{\eta}) \Big] \, \mathrm{n}_2(\mathbf{y}), \quad \mathbf{y} \in \partial\Omega \,, \quad k = 1, 2. \end{aligned} \tag{24b}$$

As for the thermal problem, we consider N_E sources, $\{\boldsymbol{\eta}^{(n)}\}_{n=\overline{1,N_E}}$, and approximate the displacement vector, $\mathbf{u}^{(\mathsf{H})}$, associated with the homogeneous equilibrium equation (13c) by a linear combination of the displacement fundamental solutions (23) with respect to these sources, i.e.

$$\mathbf{u}^{(\mathsf{H})}(\mathbf{y}) \approx \mathbf{u}^{(\mathsf{H})}_{N_E}(\mathbf{c}^{(2)}, \boldsymbol{\eta}; \mathbf{y}) = \sum_{n=1}^{N_E} \mathbf{U}(\mathbf{y}, \boldsymbol{\eta}^{(n)})\, \mathbf{c}^{(2)}_n\,, \quad \mathbf{y} \in \overline{\Omega}\,, \tag{25}$$

where $\mathbf{c}^{(2)}_n = \big(\mathrm{c}^{(2)}_{n;1}, \mathrm{c}^{(2)}_{n;2}\big) \in \mathbb{R}^2$, $n = \overline{1, N_E}$, $\mathbf{c}^{(2)} = \big(\mathbf{c}^{(2)}_1, \mathbf{c}^{(2)}_2, \ldots, \mathbf{c}^{(2)}_{N_E}\big) \in \mathbb{R}^{2N_E}$ and $\boldsymbol{\eta} \in \mathbb{R}^{2N_E}$ is a vector containing the coordinates of the sources $\{\boldsymbol{\eta}^{(n)}\}_{n=\overline{1,N_E}}$. In a similar manner, the traction vector, $\mathbf{t}^{(\mathsf{H})}$, associated with the homogeneous equilibrium equation (13b) is approximated by a linear combination of the traction fundamental solutions (24a) and (24b), namely

$$\mathbf{t}^{(\mathsf{H})}(\mathbf{y}) \approx \mathbf{t}^{(\mathsf{H})}_{N_E}(\mathbf{c}^{(2)}, \boldsymbol{\eta}; \mathbf{y}) = \sum_{n=1}^{N_E} \mathbf{T}(\mathbf{y}, \boldsymbol{\eta}^{(n)})\, \mathbf{c}^{(2)}_n\,, \quad \mathbf{y} \in \partial\Omega\,. \tag{26}$$

By collocating the corresponding boundary conditions associated with the homogeneous mechanical equilibrium equations (13b) at the points $\{\mathbf{y}^{(n)}\}_{n=\overline{1,M^1_E}}$ on the boundary Γ_1 and, eventually, $\{\mathbf{y}^{(M^1_E+n)}\}_{n=\overline{1,M^2_E}}$ on the boundary Γ_2, one obtains the following linear system of equations for the unknown coefficients $\mathbf{c}^{(2)} \in \mathbb{R}^{2N_E}$:

$$\mathbf{A}^{(22)}\, \mathbf{c}^{(2)} = \mathbf{f}^{(2)} - \mathbf{A}^{(21)}\, \mathbf{c}^{(1)}\,. \tag{27}$$

Here $\mathbf{A}^{(22)} \in \mathbb{R}^{(4M^1_E+2(d-1)M^2_E)\times 2N_E}$ is the MFS matrix associated with the homogeneous mechanical part of the inverse problem under investigation, $\mathbf{f}^{(2)} \in \mathbb{R}^{4M^1_E+2(d-1)M^2_E}$ is the right-hand side vector containing the corresponding discretised mechanical data available on Γ_1 and, eventually, Γ_2. The matrix $\mathbf{A}^{(21)} \in \mathbb{R}^{(4M^1_E+2(d-1)M^2_E)\times N_L}$ represents the coupling of the mechanical part of the inverse problem considered with its thermal part (more precisely, the influence of the thermal field on the mechanical field) according to equations (13a), (13b), (20) and (22). Again, the values $d = 2$ and $d = 1$ cover both cases investigated herein, namely Problem (A) and Problem (B), respectively.

4.4 MFS Approximation for the Inverse Thermoelasticity Problem

From equations (16)–(27), it follows that the MFS formulation for both the Cauchy problem (5), (7) and (10), and the inverse boundary value problem (5), (7) and (11) may be recast as

$$\mathbf{A}\, \mathbf{c} = \mathbf{f}\,. \tag{28a}$$

The matrix $\mathbf{A} \in \mathbb{R}^{m\times n}$ and the vectors $\mathbf{c} \in \mathbb{R}^n$ and $\mathbf{f} \in \mathbb{R}^m$ in (28a), where $m = dM^1_L + 4M^1_E + 2(d-1)M^2_E$ and $n = N_L + 2N_E$, with $d = 2$ for the Cauchy problem (5), (7) and (10), and $d = 1$ for the inverse boundary value problem (5), (7) and (11), are given by

$$\mathbf{A} = \begin{bmatrix} \mathbf{A}^{(11)} & \mathbf{0} \\ \mathbf{A}^{(21)} & \mathbf{A}^{(22)} \end{bmatrix}, \qquad \mathbf{c} = \begin{pmatrix} \mathbf{c}^{(1)} \\ \mathbf{c}^{(2)} \end{pmatrix}, \qquad \mathbf{f} = \begin{pmatrix} \mathbf{f}^{(1)} \\ \mathbf{f}^{(2)} \end{pmatrix}. \tag{28b}$$

Clearly, once the MFS coefficients $\mathbf{c}^{(1)} \in \mathbb{R}^{N_L}$ and $\mathbf{c}^{(2)} \in \mathbb{R}^{2N_E}$ have been determined by solving the system of linear equations (28a), the approximations for the unknown elastic fields are obtained using the superposition principle together with equations (20), (22), (25) and (26).

5 Regularization

To uniquely determine the solution $\mathbf{c} \in \mathbb{R}^{N_L+2N_E}$ of the system of equations (28a), the numbers of boundary collocation points and sources must satisfy the inequality $dM^1_L + 4M^1_E + 2(d-1)M^2_E \geq$

$N_L + 2N_E$. In practice, the same collocation points and sources are used for both the thermal and the mechanical problems, i.e. $\{\mathbf{x}^{(m)}\}_{m=\overline{1,M_L}} = \{\mathbf{y}^{(m)}\}_{m=\overline{1,M_E}}$ with $M_L = M_E =: M$ and $\{\boldsymbol{\xi}^{(n)}\}_{n=\overline{1,N_L}} = \{\boldsymbol{\eta}^{(n)}\}_{n=\overline{1,N_E}}$ with $N_L = N_E =: N$, respectively. Consequently, the inequality that ensures the uniqueness of the solution of the system of equations (28a) reduces to $(d+4)M_1 + 2(d-1)M_2 \geq 3N$, where $M_j := M_L^j = M_E^j$, $j = 1, 2$.

5.1 SVD-Based Regularization Methods

Since the inverse problems (A) and (B) under investigation are ill-posed, the system of equations (28a) is ill-conditioned and hence it cannot be solved by direct methods, such as the least-squares method, because such an approach would produce a highly unstable solution for noisy data on Γ_1 and/or Γ_2. This fact can be simply viewed from the SVD of the system matrix $\mathbf{A} \in \mathbb{R}^{m\times n}$, $m \geq n$, which is a decomposition of the form [37]

$$\mathbf{A} = \mathbf{U}\,\boldsymbol{\Sigma}\,\mathbf{V}^{\mathsf{T}} = \sum_{i=1}^{n} \mathbf{u}_i\,\sigma_i\,\mathbf{v}_i^{\mathsf{T}}, \tag{29}$$

where $\mathbf{U} = [\mathbf{u}_1, \mathbf{u}_2, \ldots \mathbf{u}_m] \in \mathbb{R}^{m\times m}$ and $\mathbf{V} = [\mathbf{v}_1, \mathbf{v}_2, \ldots \mathbf{v}_n] \in \mathbb{R}^{n\times n}$ are orthogonal matrices whose columns are the left and right singular vectors $\mathbf{u}_i$ and $\mathbf{v}_i$ of $\mathbf{A}$, respectively, and $\boldsymbol{\Sigma} = \operatorname{diag}(\sigma_1, \sigma_2, \ldots, \sigma_n) \in \mathbb{R}^{n\times n}$ is a diagonal matrix whose diagonal elements are the non-negative singular values of $\mathbf{A}$ appearing in a non-increasing order, i.e. $\sigma_1 \geq \sigma_2 \geq \ldots \geq \sigma_n \geq 0$.

By using the SVD (29), the least-squares solution $\mathbf{c}^{(\mathsf{LS})}$ of system (28a) is obtained as

$$\mathbf{c}^{(\mathsf{LS})} = \sum_{i=1}^{n} \frac{\mathbf{u}_i^{\mathsf{T}}\,\mathbf{b}}{\sigma_i}\,\mathbf{v}_i. \tag{30}$$

The above relation clearly shows that the least-squares solution (30) is unstable and oscillatory if singular values become small. To overcome this and obtain a stable solution, the contributions of the small singular values to the least-squares solution (30) of (28a) need be filtered out and this is achieved by employing a regularization method. The standard non-iterative regularization techniques usually associated with the SVD and the corresponding regularized solutions of the system of equations (28a) are the following [37]:

(R1) The TRM provides a regularized solution $\mathbf{c}_\lambda^{(\mathsf{TRM})} \in \mathbb{R}^n$ as the solution of the following minimization problem:

$$\min_{\mathbf{c}\in\mathbb{R}^n} \Big\{ \|\mathbf{A}\mathbf{c} - \mathbf{f}\|_2^2 + \lambda^2 \|\mathbf{c}\|_2^2 \Big\}, \tag{31}$$

where $\lambda > 0$ is a regularization parameter to be prescribed. Based on the SVD, this TRM solution can be written in the form

$$\mathbf{c}_\lambda^{(\mathsf{TRM})} = \sum_{i=1}^{n} \phi_i^{(\mathsf{TRM})}\,\frac{\mathbf{u}_i^{\mathsf{T}}\,\mathbf{b}}{\sigma_i}\,\mathbf{v}_i, \quad \text{where} \quad \phi_i^{(\mathsf{TRM})} = \frac{\sigma_i^2}{\sigma_i^2 + \lambda^2}, \quad i = \overline{1,n}. \tag{32}$$

(R2) The DSVD solution $\mathbf{c}_\lambda^{(\mathsf{DSVD})} \in \mathbb{R}^n$ has an expression similar to the TRM solution (32), but with different filter factors, namely

$$\mathbf{c}_\lambda^{(\mathsf{DSVD})} = \sum_{i=1}^{n} \phi_i^{(\mathsf{DSVD})}\,\frac{\mathbf{u}_i^{\mathsf{T}}\,\mathbf{b}}{\sigma_i}\,\mathbf{v}_i, \quad \text{where} \quad \phi_i^{(\mathsf{DSVD})} = \frac{\sigma_i}{\sigma_i + \lambda}, \quad i = \overline{1,n}, \tag{33}$$

where the regularization parameter $\lambda > 0$ is to be prescribed. We note that the DSVD filter factors defined in (33) decay slower than the TRM filter factors given by (32) and, consequently, the DSVD introduces less filtering than the TRM.

(R3) In the case of the TSVD, the original ill-conditioned MFS matrix $\mathbf{A}$ is considered as a noisy representation of a mathematically rank-deficient matrix and is replaced by a well-conditioned rank-deficient matrix that is close to $\mathbf{A}$. The standard choice for this approach is to consider the closest rank$-k$ approximation $\mathbf{A}_k$ to the original matrix $\mathbf{A}$, with respect to the Euclidean norm, by truncating the SVD expression (29) at $k \leq n$, namely

$$\mathbf{A}_k = \sum_{i=1}^{k} \mathbf{u}_i \, \sigma_i \, \mathbf{v}_i^{\mathsf{T}}, \tag{34}$$

which in turn it produces the truncated solution of (30) as

$$\mathbf{c}_k^{(\mathsf{TSVD})} = \sum_{i=1}^{k} \frac{\mathbf{u}_i^{\mathsf{T}} \, \mathbf{b}}{\sigma_i} \, \mathbf{v}_i. \tag{35}$$

We note that the truncation number k is the regularization parameter for the TSVD. It should be mentioned that the TSVD solution (35) can also be expressed analogously to the TRM and DSVD solutions given by equations (32) and (33), respectively, by defining the corresponding filter factors $\phi_i^{(\mathsf{TSVD})}$, $i = \overline{1,n}$, namely

$$\mathbf{c}_k^{(\mathsf{TSVD})} = \sum_{i=1}^{n} \phi_i^{(\mathsf{TSVD})} \, \frac{\mathbf{u}_i^{\mathsf{T}} \, \mathbf{b}}{\sigma_i} \, \mathbf{v}_i, \quad \text{where} \quad \phi_i^{(\mathsf{TSVD})} = \begin{cases} 1\,, & i = \overline{1,k} \\ 0\,, & i = \overline{(k+1),n}\,. \end{cases} \tag{36}$$

5.2 Criteria for Selecting the Regularization Parameter

It is well-known that the performance of regularization methods depends crucially on the choice of the regularization parameter λ, with the convention that λ denotes the truncation number k for the TSVD. The criteria available in the literature and usually employed for the selection of the regularization parameter are, generally speaking, either mathematically rigorous or heuristic. Any rigorous criterion requires a reliable estimation of the amount of noise present in the data, whereas the latter approaches, although heuristic, may be practically useful in cases when no a priori information about the amount of noise is available.

In this study, we employ the following criteria to select the regularization parameter for the regularization methods (R1)–(R3):

(C1) The *L–curve criterion* (LC) [37, 40] is a heuristic approach stating that the regularization parameter λ_{LC} can be chosen at the corner (i.e. the point of maximum curvature) of the following curve:

$$\Big\{ \big(\log \|\mathbf{A}\,\mathbf{c}_\lambda - \mathbf{f}^\varepsilon\|_2, \log \|\mathbf{c}_\lambda\|_2 \big) \;\Big|\; \lambda > 0 \Big\}, \tag{37}$$

where $\mathbf{f}^\varepsilon$ represents a noisy perturbation of the exact data $\mathbf{f}$.

(C2) The *discrepancy principle* (DP) of [38] is mathematically rigorous, however it requires a reliable estimation of the amount of noise ε present in the data, i.e.

$$\|\mathbf{f}^\varepsilon - \mathbf{f}\|_2 \leq \varepsilon \quad \Longrightarrow \quad \lambda_{\mathsf{DP}} = \max \Big\{ \lambda > 0 \;\Big|\; \|\mathbf{A}\,\mathbf{c}_\lambda - \mathbf{f}^\varepsilon\|_2 \leq \varepsilon \Big\}. \tag{38}$$

(C3) The *generalized cross-validation* (GCV) *criterion* [39] is based on the following ideas: (i) if an arbitrary element, f_i, $i \in \overline{1,m}$, of the right-hand side $\mathbf{f}$ is left out, then the corresponding regularized solution should predict this observation well; and (ii) the choice of the regularization parameter should be independent of an orthogonal transformation of $\mathbf{f}$. Hence the selection of the regularization parameter λ_{GCV} is realised by minimizing the GCV function

$$\mathscr{G}(\cdot) : (0,\infty) \longrightarrow [0,\infty), \quad \mathscr{G}(\lambda) = \frac{\|\mathbf{A}\,\mathbf{c}_\lambda - \mathbf{f}^\varepsilon\|_2^2}{[\mathrm{tr}(\mathbf{I}_m - \mathbf{A}\,\mathbf{A}^\dagger)]^2}\,, \tag{39}$$

where $\mathbf{A}^{\dagger}$ is the matrix that provides the regularized solution when multiplied with the perturbed right-hand side $\mathbf{f}^{\varepsilon}$, i.e.

$$\mathbf{c}_{\lambda} = \mathbf{A}^{\dagger}\,\mathbf{f}^{\varepsilon}, \qquad \mathbf{A}^{\dagger} \equiv \left(\mathbf{A}^{\mathsf{T}}\mathbf{A} + \lambda^2 \mathbf{I}_n\right)^{-1}\mathbf{A}^{\mathsf{T}}. \tag{40}$$

6 Numerical Results

We apply the numerical procedure described in Section 3, using the MFS-MPS presented in Section 4 together with the non-iterative regularization methods and the stopping criteria briefly described in Sections 5.1 and 5.2, respectively, to three test problems. More precisely, we solve the inverse problems (A) and (B) in both simply and doubly connected two-dimensional domains with either a smooth or a partially smooth boundary, for an isotropic linear thermoelastic material (copper alloy) characterised by the material constants $G = 4.80\times10^{10}\,\mathrm{N/m^2}$, $\nu = 0.34$, $\kappa = 4.01\,\mathrm{W\,m^{-1}\,K^{-1}}$ and $\alpha_{\mathrm{T}} = 16.5\times10^{-6}\,{}^{\circ}\mathrm{C}^{-1}$.

Example 1 (simply connected domain, smooth boundary): We consider the inverse boundary value problem (B) in the unit disk $\Omega = \left\{\mathbf{x}\in\mathbb{R}^2 \,\middle|\, \|\mathbf{x}\| < \mathrm{R}\right\}$, $\mathrm{R} = 1.0$, and the analytical solution (plane strain state) given by equations (14a), (14b) and (15a)–(15c), with $K = 2$, $\mathbf{x}^{(1)} = (5.0, 5.0)$, $\mathbf{x}^{(2)} = (-2.0, 4.0)$, $\mathrm{T}_1 = 5{}^{\circ}\mathrm{C}$ and $\mathrm{T}_2 = -1{}^{\circ}\mathrm{C}$. Here, we consider $\Gamma_1 = \left\{\mathbf{x}\in\mathbb{R}^2 \,\middle|\, \|\mathbf{x}\| = \mathrm{R},\, \theta\in[0,\theta_0]\right\}$ and $\Gamma_2 = \left\{\mathbf{x}\in\mathbb{R}^2 \,\middle|\, \|\mathbf{x}\| = \mathrm{R},\, \theta\in(\theta_0,2\pi)\right\}$, where $\theta = \theta(\mathbf{x})$ is the radial angular polar coordinate of the point $\mathbf{x}\in\mathbb{R}^2$ and $\theta_0 \in \left\{2\pi/3, \pi, 4\pi/3\right\}$.

Example 2 (doubly connected domain, smooth boundary): We consider the Cauchy problem (A) in the annular domain $\Omega = \left\{\mathbf{x}\in\mathbb{R}^2 \,\middle|\, \mathrm{R_{int}} < \|\mathbf{x}\| < \mathrm{R_{out}}\right\}$, where $\mathrm{R_{int}} = 1.0$ and $\mathrm{R_{out}} = 2.0$, which is bounded by the inner and outer boundaries $\Gamma_{\mathrm{int}} = \left\{\mathbf{x}\in\mathbb{R}^2 \,\middle|\, \|\mathbf{x}\| = \mathrm{R_{int}}\right\}$ and $\Gamma_{\mathrm{out}} = \left\{\mathbf{x}\in\mathbb{R}^2 \,\middle|\, \|\mathbf{x}\| = \mathrm{R_{out}}\right\}$, respectively. We also assume that the thermoelastic fields associated with the Example 2 correspond to constant inner and outer temperatures, $\mathrm{T_{int}} = 1{}^{\circ}\mathrm{C}$ and $\mathrm{T_{out}} = 10{}^{\circ}\mathrm{C}$, as well as constant inner and outer radial pressures, $\sigma_{\mathrm{int}} = 1.0\times10^{10}\,\mathrm{N/m^2}$ and $\sigma_{\mathrm{out}} = 2.0\times10^{10}\,\mathrm{N/m^2}$, respectively, which describe a plane strain state. The analytical solution of this problem is:

$$\mathrm{T}^{(\mathrm{an})}(\mathbf{x}) = \mathrm{T_{out}}\,\frac{\log\left(\|\mathbf{x}\|/\mathrm{R_{int}}\right)}{\log\left(\mathrm{R_{out}}/\mathrm{R_{int}}\right)} + \mathrm{T_{int}}\,\frac{\log\left(\mathrm{R_{out}}/\|\mathbf{x}\|\right)}{\log\left(\mathrm{R_{out}}/\mathrm{R_{int}}\right)}, \quad \mathbf{x}\in\overline{\Omega}, \tag{41a}$$

$$\mathrm{q}^{(\mathrm{an})}(\mathbf{x}) = -\kappa\,\frac{\mathrm{T_{out}} - \mathrm{T_{int}}}{\log\left(\mathrm{R_{out}}/\mathrm{R_{int}}\right)}\,\frac{\mathbf{x}\cdot\mathbf{n}(\mathbf{x})}{\|\mathbf{x}\|^2}, \quad \mathbf{x}\in\partial\Omega, \tag{41b}$$

$$\mathbf{u}^{(\mathrm{an})}(\mathbf{x}) = \left[\frac{\gamma}{2}\left(\frac{1-2\nu}{1-\nu}\right)\frac{\mathrm{T_{out}} - \mathrm{T_{int}}}{\log\left(\mathrm{R_{out}}/\mathrm{R_{int}}\right)}\,\log\|\mathbf{x}\| + \mathsf{V}\left(\frac{1-\nu}{1+\nu}\right) - \mathsf{W}\,\frac{1}{\|\mathbf{x}\|^2}\right]\frac{\mathbf{x}}{2G}, \quad \mathbf{x}\in\overline{\Omega}, \tag{41c}$$

$$\mathbf{t}^{(\mathrm{an})}(\mathbf{x}) = \begin{cases} -\sigma_{\mathrm{out}}\,\mathbf{n}(\mathbf{x}), & \mathbf{x}\in\Gamma_{\mathrm{out}} \equiv \left\{\mathbf{x}\in\partial\Omega \,\middle|\, \|\mathbf{x}\| = \mathrm{R_{out}}\right\} \\ -\sigma_{\mathrm{int}}\,\mathbf{n}(\mathbf{x}), & \mathbf{x}\in\Gamma_{\mathrm{int}} \equiv \left\{\mathbf{x}\in\partial\Omega \,\middle|\, \|\mathbf{x}\| = \mathrm{R_{int}}\right\}, \end{cases} \tag{41d}$$

where

$$\mathsf{V} \equiv -\frac{\sigma_{\mathrm{out}}^{(\mathsf{H})}\,\mathrm{R_{out}^2} - \sigma_{\mathrm{int}}^{(\mathsf{H})}\,\mathrm{R_{int}^2}}{\mathrm{R_{out}^2} - \mathrm{R_{int}^2}}, \qquad \mathsf{W} \equiv \frac{\left(\sigma_{\mathrm{out}}^{(\mathsf{H})} - \sigma_{\mathrm{int}}^{(\mathsf{H})}\right)\mathrm{R_{out}^2}\,\mathrm{R_{int}^2}}{\mathrm{R_{out}^2} - \mathrm{R_{int}^2}}, \tag{42a}$$

$$\sigma_{\mathrm{out}}^{(\mathsf{H})} \equiv \sigma_{\mathrm{out}} - \gamma\,\mathrm{T_{out}} + \frac{\gamma}{2}\,\frac{\mathrm{T_{out}} - \mathrm{T_{int}}}{\log\left(\mathrm{R_{out}}/\mathrm{R_{int}}\right)}\left(\frac{1}{1-\nu}\,\log\mathrm{R_{out}} + 1\right), \tag{42b}$$

and

$$\sigma_{\rm int}^{(\mathsf{H})} \equiv \sigma_{\rm int} - \gamma\, {\rm T}_{\rm int} + \frac{\gamma}{2}\, \frac{{\rm T}_{\rm out} - {\rm T}_{\rm int}}{\log\left({\rm R}_{\rm out}/{\rm R}_{\rm int}\right)} \left(\frac{1}{1-\nu}\, \log {\rm R}_{\rm int} + 1 \right). \tag{42c}$$

Here $\Gamma_1 = \Gamma_{\rm out}$ and $\Gamma_2 = \Gamma_{\rm int}$.

Example 3 (simply connected domain, piecewise smooth boundary): We consider the inverse boundary value problem (B) in the square $\Omega = (-0.5, 0.5)^2$, with the analytical solution (plane strain state) given by equations (14a), (14b) and (15a)–(15c), with $K = 2$, $\mathbf{x}^{(1)} = (8.0, 8.0)$, $\mathbf{x}^{(2)} = (5.0, -1.0)$, ${\rm T}_1 = 100°{\rm C}$ and ${\rm T}_2 = 50°{\rm C}$. Here, we consider $\Gamma_1 = [-0.5, 0.5] \times \big\{ \pm 0.5 \big\} \cup \big\{ 0.5 \big\} \times (-0.5, 0.5)$ and $\Gamma_2 = \big\{ -0.5 \big\} \times (-0.5, 0.5)$.

In all examples we have taken $M_L^j = M_E^j = M_j$ uniformly distributed collocation points on Γ_j, $j = 1, 2$, such that $M_1 + M_2 = M$. Also, we take $N_L = N_E = N$ uniformly distributed sources associated with both the over- and under-specified boundaries Γ_1 and Γ_2, respectively. Moreover, the sources are preassigned and kept fixed throughout the solution process (i.e. the so-called static MFS approach has been employed) on a pseudo-boundary $\partial\widetilde{\Omega}$ of a similar shape to that of $\partial\Omega$ such that $\mathrm{dist}\big(\partial\widetilde{\Omega}, \partial\Omega\big)$ is a fixed constant [42]. According to the notations used in Section 4, the corresponding MFS parameters have been set as follows:

(i) **Example 1:** $N = 42$ on $\partial\widetilde{\Omega} = \Big\{ \mathbf{x} \in \mathbb{R}^2 \,\Big|\, \|\mathbf{x}\| = {\rm R} + {\rm d} \Big\}$, where ${\rm d} = 2.0$ and $M = (\ell + 1)N/6$ on Γ_1, for $\theta_0 = (\ell + 1)\pi/3$ and $\ell \in \big\{1, 2, 3\big\}$.

(ii) **Example 2:** $M_1 = 40$ on Γ_1, $N_1 = 40$ and $N_2 = 20$ on $\widetilde{\Gamma}_{\rm out} = \Big\{ \mathbf{x} \in \mathbb{R}^2 \,\Big|\, \|\mathbf{x}\| = {\rm R}_{\rm out} + {\rm d}_1 \Big\}$ and $\widetilde{\Gamma}_{\rm int} = \Big\{ \mathbf{x} \in \mathbb{R}^2 \,\Big|\, \|\mathbf{x}\| = {\rm R}_{\rm int} - {\rm d}_2 \Big\}$, respectively, such that $N = N_1 + N_2$, where $\partial\widetilde{\Omega} = \widetilde{\Gamma}_{\rm out} \cup \widetilde{\Gamma}_{\rm int}$, ${\rm d}_1 = 2.0$ and ${\rm d}_2 = 0.5$.

(iii) **Example 3:** $N = 40$ on $\partial\widetilde{\Omega} = \big[-0.5-{\rm d}, 0.5+{\rm d}\big] \times \big\{\pm(0.5+{\rm d})\big\} \cup \big\{\pm(0.5+{\rm d})\big\} \times \big[-0.5-{\rm d}, 0.5+{\rm d}\big]$, where ${\rm d} = 2.0$ and $M_1 = 3N/4$ on Γ_1.

In order to simulate the inherent measurement errors, we consider that the boundary data corresponding to the inverse problems investigated herein is noisy. More precisely, we assume that the given exact boundary data $\widetilde{\rm F}\big|_{\Gamma_1} = {\rm F}^{(\rm an)}\big|_{\Gamma_1}$ or, eventually, $\widetilde{\rm F}\big|_{\partial\Omega} = {\rm F}^{(\rm an)}\big|_{\partial\Omega}$ has been perturbed as

$$\widetilde{\rm F}^{\varepsilon}(\mathbf{x}) = \big(1 + {\rm p_F}\rho\big)\, {\rm F}^{(\rm an)}(\mathbf{x}), \quad \mathbf{x} \in \Gamma, \tag{43}$$

where $\Gamma = \Gamma_1$ or $\Gamma = \partial\Omega$, ${\rm p_F}$ is the percentage noise and ρ is a pseudo-random number drawn from the standard uniform distribution on the interval [-1, 1] generated using the MATLAB command $-1 + 2 * \mathsf{rand}(\cdot)$. It should be mentioned that, for the inverse problems with noisy boundary data considered, the accuracy of the numerical results was found to be quite insensitive with respect to the location of the MFS pseudo-boundary. For all examples considered, the L-curves (37), the DP curves (38) and the GCV functions (39), as well as the calculation of the corresponding values of the regularization parameters, were carried out using the MATLAB routines available in Hansen's regularization tools package [43, 44].

Further, to assess the accuracy and convergence of the combined MFS-MPS approach and SVD-based regularizing methods (R1)–(R3) in conjunction with the selection criteria (C1)–(C3), for any real-valued function $f : \Gamma \longrightarrow \mathbb{R}$, where $\Gamma = \Gamma_2$ or $\Gamma = \partial\Omega$, and any set of points $\big\{\mathbf{x}^{(n)}\big\}_{n=\overline{1,N_\Gamma}} \subset \Gamma$, we introduce the following *relative root mean square* (*RMS*) *error* of f on Γ:

$$\mathrm{e}_\Gamma(f) = \sqrt{\frac{1}{N_\Gamma} \sum_{n=1}^{N_\Gamma} \Big[f^{(\rm num)}\big(\mathbf{x}^{(n)}\big) - f\big(\mathbf{x}^{(n)}\big) \Big]^2} \Bigg/ \sqrt{\frac{1}{N_\Gamma} \sum_{n=1}^{N_\Gamma} f\big(\mathbf{x}^{(n)}\big)^2}\,, \tag{44a}$$

where $f^{(\mathrm{num})}(\mathbf{x})$ denotes an approximate numerical value for $f(\mathbf{x})$, $\mathbf{x} \in \Gamma$. To investigate the local accuracy of the numerical solution, one could also employ the following *pointwise normalized error* of f at $\mathbf{x} \in \Gamma$:

$$\mathrm{E}_f(\mathbf{x}) = \frac{\left|f^{(\mathrm{num})}(\mathbf{x}) - f(\mathbf{x})\right|}{\max_{\mathbf{y}\in\Gamma}\left|f(\mathbf{y})\right|}, \quad \mathbf{x} \in \Gamma\,. \tag{44b}$$

Table 1 presents the values of the regularization parameter and the corresponding RMS errors, $\mathrm{e}_{\Gamma_2}(\mathrm{T})$, $\mathrm{e}_{\partial\Omega}(\mathrm{q})$ and $\mathrm{e}_{\Gamma_2}(\mathbf{u})$, obtained using the non-iterative regularization methods (R1)–(R3), the criteria (C1)–(C3) and various amounts of noise added to the data (11a)–(11c), for the inverse problem given by Example 1 with $\theta_0 = \pi$, i.e. $\mathrm{meas}(\Gamma_1)/\mathrm{meas}(\Gamma_2) = 1$. It can be seen from this table that each of the regularization methods (R1)–(R3) has a stabilising/regularizing effect on the numerical solution of the inverse boundary value problem (B), provided that an appropriate criterion is employed for the selection of the regularization parameter λ or the truncation number k. More precisely, both the LC and the DP are suitable criteria for the regularization methods (R1)–(R3), whilst the GCV fails to provide a good value for λ or k and hence a corresponding accurate solution for Example 1. The best combinations, in terms of the accuracy, for the numerical solution of Example 1, are TRM-LC, DSVD-LC and TSVD-DP, and these are displayed in Figs. 1–3, respectively. From these figures, as well as Table 1, one can conclude that the numerical solutions of Problem (B) for Example 1 obtained using these methods are all very accurate and stable with respect to decreasing the amount of noise in the data.

Similar conclusions regarding the suitability of both the LC and the DP for providing good values of the regularization parameter also hold if one considers Example 1 with $\theta_0 = 4\pi/3$ $\big(\mathrm{meas}(\Gamma_1)/\mathrm{meas}(\Gamma_2) > 1\big)$ or $\theta_0 = 2\pi/3$ $\big(\mathrm{meas}(\Gamma_1)/\mathrm{meas}(\Gamma_2) < 1\big)$. The numerically retrieved solutions of the inverse problem (5), (7) and (11a)–(11c), using (R1)-(R3) in conjunction with the criteria (C1)–(C3), and $\mathrm{p_T} = \mathrm{p_u} = \mathrm{p_t} \in \{1\%, 3\%, 5\%\}$, for Example 1 with $\theta_0 = 4\pi/3$ and $\theta_0 = 2\pi/3$, are presented in Figs. 4–6 and Figs. 7–9, respectively. Although the length of the boundary Γ_1 on which both the temperature and the displacement vector are prescribed decreases as θ_0 decreases, not only the numerical solutions obtained via the TRM-LC, DSVD-LC and TSVD-DP remain stable, but they are also good approximations for their corresponding exact counterparts, see Figs. 1–9. The values of λ or k and the corresponding RMS errors, $\mathrm{e}_{\Gamma_2}(\mathrm{T})$, $\mathrm{e}_{\partial\Omega}(\mathrm{q})$ and $\mathrm{e}_{\Gamma_2}(\mathbf{u})$, obtained using methods (R1)–(R3) with the best criteria (C1)–(C3) and various amounts of noise in the data (11a)–(11c), for Example 1 with $\theta_0 \in \big\{2\pi/3, \pi, 4\pi/3\big\}$, are given in Table 2.

The TRM, DSVD and TSVD also produce accurate and stable numerical solutions for Problem (A) in a doubly connected domain with a smooth boundary such as the annular domain considered in Example 2. Table 3 presents the values of λ or k and the corresponding RMS errors, $\mathrm{e}_{\Gamma_2}(\mathrm{T})$, $\mathrm{e}_{\Gamma_2}(\mathrm{q})$, $\mathrm{e}_{\Gamma_2}(\mathbf{u})$ and $\mathrm{e}_{\Gamma_2}(\mathbf{t})$, obtained using the regularization methods (R1)–(R3), the criteria (C1)–(C3) and various amounts of noise in the data (10a)–(10b), for Example 2. As shown in Table 3, the criteria (C1)–(C3) are all suitable for the TRM and DSVD, whilst the TSVD produces accurate and stable numerical solutions for Example 2 in conjunction with the DP and GCV only, with the mention that the latter criterion fails to produce accurate results when increasing the level of noise in the Cauchy data on Γ_1. The exact and numerical solutions for the thermal and mechanical fields on the boundary Γ_2, retrieved using the TRM-LC, DSVD-LC and TSVD-DP, for noisy data $\mathrm{p_T} = \mathrm{p_u} \in \{1\%, 3\%, 5\%\}$ on Γ_1, are displayed in Figs. 10–12, respectively.

Also for Problem (B) in a simply connected domain with a piecewise smooth boundary considered in Example 3, stable and accurate results have been obtained for $\mathrm{T}\big|_{\Gamma_2}$, $\mathrm{q}\big|_{\partial\Omega}$ and $\mathbf{u}\big|_{\Gamma_2}$, using the TRM and DSVD in conjunction with the LC, GCV and DP, whilst the same conclusion holds if the TSVD is employed together with the GCV and DP only. These numerical reconstructions for the unknown boundary temperature and displacement vector on Γ_2, and the unknown normal heat flux on $\partial\Omega = \Gamma_1 \cup \Gamma_2$, obtained using the TRM-LC, DSVD-LC and TSVD-DP are presented in Figs. 13–15, respectively, together with their corresponding exact values on the side $\mathrm{x}_1 = -0.5$. The corresponding

values of λ or k and the associated RMS errors, $\mathrm{e}_{\Gamma_2}(\mathrm{T})$, $\mathrm{e}_{\partial\Omega}(\mathrm{q})$ and $\mathrm{e}_{\Gamma_2}(\mathbf{u})$, obtained using methods (R1)–(R3), the criteria (C1)–(C3) and various levels of noise in the boundary data $\mathbf{u}\big|_{\Gamma_1}$ and $\mathbf{t}\big|_{\Gamma_1}$ are tabulated in Table 4.

Finally, we investigate the sensitivity of the numerical results obtained using methods (R1)–(R3), together with the criteria (C1)–(C3), with respect to the distance between the boundary $\partial\Omega$ and the pseudo-boundary $\partial\widetilde{\Omega}$ on which the sources are located, i.e. $\mathrm{d} = \mathrm{dist}\big(\partial\widetilde{\Omega}, \partial\Omega\big)$. To do so, we consider the inverse boundary value problem given by Example 1 with $\theta_0 = \pi$, set $N = 42$ sources on $\partial\widetilde{\Omega} = \Big\{\mathbf{x} \in \mathbb{R}^2 \,\Big|\, \|\mathbf{x}\| = \mathrm{R} + \mathrm{d}\Big\}$, $M = N/2$ collocation points on Γ_1 and $\mathrm{p}_{\mathrm{T}} = \mathrm{p}_{\mathbf{u}} = 1\%$, and vary $\mathrm{d} \in (0, 10]$. Figs. 16(a)–16(c) present the RMS errors $\mathrm{e}_{\Gamma_2}(\mathrm{T})$, $\mathrm{e}_{\partial\Omega}(\mathrm{q})$ and $\mathrm{e}_{\Gamma_2}(\mathbf{u})$, as functions of the distance d, obtained using the TRM-LC, DSVD-LC and TSVD-DP, respectively. As expected, all the RMS errors decrease with respect to increasing d and then they stabilise reaching a plateau region.

7 Conclusions

We have investigated the reconstruction of the missing thermal and mechanical data on an inaccessible part of the boundary for two-dimensional linear isotropic thermoelastic materials from over-prescribed noisy measurements taken on the remaining accessible boundary part. Two types of inverse problems, namely equations (5) and (7) together with either (10) or (11), were solved by employing the MFS in conjunction with the method of particular solutions. The stabilisation/regularization of the inverse boundary value problems considered was achieved by using several SVD-based regularization methods, such as the TRM [36], the DSVD and the TSVD [37], while the regularization parameter or the truncation number was chosen according to the DP [38], GCV criterion [39] and Hansen's LC method [40]. The following major conclusions have been drawn from the present study:

(i) All three regularization methods (R1)–(R3) provide us with a stable solution of the inverse boundary value problems (A) and (B), provided that a suitable criterion for the selection of the regularization parameter is used.

(ii) For the inverse boundary value problem (B) in a two-dimensional simply connected domain with a smooth boundary considered in Example 1, both the LC and the DP are suitable criteria for all three regularization methods, whilst the GCV fails to provide an optimal value for all these methods.

(iii) In the case of inverse problems in a two-dimensional doubly connected domain with a smooth boundary (Example 2), or a two-dimensional simply connected domain with a piecewise smooth boundary (Example 3), a stable and accurate numerical solution is obtained if the TRM and DSVD are combined with any of the criteria (C1)–(C3), or the TSVD is employed together with either the GCV or the DP.

The extension of the present work to inverse boundary value problems in three-dimensional isotropic linear thermoelasticity is currently under investigation.

Acknowledgements. The financial support received from the Romanian National Authority for Scientific Research (CNCS–UEFISCDI), project number PN–II–ID–PCE–2011–3–0521, is gratefully acknowledged.

References

[1] W. Nowacki, *Thermoelasticity*. Pergamon Press, Oxford, 1986.

[2] A. H.–D. Cheng, C. S. Chen, M. A. Golberg, and Y. F. Rashed, BEM for thermoelasticity and elasticity with body force – a revisit, *Engineering Analysis with Boundary Elements* 25 (2001), 377–387.

[3] N. Kamiya, Y. Aikawa, and K. Kawaguchi, An adaptive boundary element scheme for steady thermoelastic analysis, *Computer Methods in Applied Mechanics and Engineering* 119 (1994), 311–324.

[4] F. J. Rizzo and D. J. Shippy, An advanced boundary integral equation method for three-dimensional thermoelasticity, *International Journal for Numerical Methods in Engineering* 11 (1977), 1753–1768.

[5] V. Sladek and J. Sladek, Boundary integral equation in thermoelasticity. Part I: General analysis, *Applied Mathematical Modelling* 7 (1983), 413–418.

[6] V. Sladek and J. Sladek, Boundary integral equation in thermoelasticity. Part III: Uncoupled thermoelasticity, *Applied Mathematical Modelling* 8 (1984), 413–418.

[7] P. W. Partridge, C. A. Brebbia, and L. C. Wrobel, *The Dual Reciprocity Boundary Element Method*. Computational Mechanics Publications, Southampton, 1992.

[8] B. H. Dennis and G. S. Dulikravich, "A finite element formulation for the detection of boundary conditions in elasticity and heat conduction," in *Inverse Problems in Engineering Mechanics*, M. Tanaka and G. S. Dulikravich (Editors), Elsevier Science BV, UK, 1998, pp. 61–70.

[9] B. H. Dennis and G. S. Dulikravich, Simultaneous determination of temperatures, heat fluxes, deformations, and tractions on inaccessible boundaries, *Journal of Heat Transfer, Transactions of the ASME* 121 (1999), 537–545.

[10] J. Sladek, V. Sladek, and S. N. Atluri, A pure contour formulation for the meshless local boundary integral equation method in thermoelasticity, *CMES–Computer Modeling in Engineering and Science* 2 (2001), 423–433.

[11] A. Karageorghis and Y.–S. Smyrlis, Matrix decomposition MFS algorithms for elasticity and thermo-elasticity problems in axisymmetric domains, *Journal of Computational and Applied Mathematics* 206 (2007), 774–795.

[12] L. Marin and A. Karageorghis, The MFS–MPS for two-dimensional steady-state thermoelasticity problems, *Engineering Analysis with Boundary Elements* 37 (2013), 1004–1020.

[13] C. C. Tsai, The method of fundamental solutions with dual reciprocity for three-dimensional thermoelasticity under arbitrary forces, *International Journal for Computer-Aided Engineering and Software* 26 (2009), 229–244.

[14] J. Hadamard, *Lectures on Cauchy's Problem in Linear Partial Differential Equations*. Yale University Press, Hew Haven, 1923.

[15] E. Trefftz, "Ein Gegenstück zum Ritzschen Verfahren," in *Verhandlungen des 2. Internationalen Kongresses für Technische Mechanik*, Zürich, Switzerland, 1926, pp. 131–137.

[16] E. Kita and N. Kamiya, Trefftz method: An overview, *Advances in Engineering Software* 24 (1995), 3–12.

[17] R. Mathon and R. L. Johnston, The approximate solution of elliptic boundary value problems by fundamental solutions, *SIAM Journal on Numerical Analysis* 14 (1977), 638–650.

[18] G. Fairweather and A. Karageorghis, The method of fundamental solutions for elliptic boundary value problems, *Advances in Computational Mathematics* 9 (1998), 69–95.

[19] G. Fairweather, A. Karageorghis, and P. A. Martin, The method of fundamental solutions for scattering and radiation problems, *Engineering Analysis with Boundary Elements* 27 (2003), 759–769.

[20] M. A. Golberg and C. S. Chen, "The method of fundamental solutions for potential, Helmholtz and diffusion problems," in *Boundary Integral Methods: Numerical and Mathematical Aspects*, M. A. Golberg (Editor), Computational Engineering, vol. 1, WIT Press/Computational Mechanics Publications, Boston, MA, 1999, pp. 103176.

[21] A. Karageorghis, D. Lesnic, and L. Marin, A survey of applications of the MFS to inverse problems, *Inverse Problems in Science and Engineering* 19 (2011), 309–336.

[22] Y. C. Hon and T. Wei, A fundamental solution method for inverse heat conduction problems, *Engineering Analysis with Boundary Elements* 28 (2004), 489–495.

[23] Y. C. Hon and T. Wei, The method of fundamental solutions for solving multidimensional heat conduction problems, *CMES: Computer Modeling in Engineering & Sciences* 13 (2005), 219–228.

[24] L. Marin, The method of fundamental solutions for inverse problems associated with the steady-state heat conduction in the presence of sources, *CMES: Computer Modeling in Engineering & Sciences* 30 (2008), 99–122.

[25] T. Wei, Y. C. Hon, and L. Ling, Method of fundamental solutions with regularization techniques for Cauchy problems of elliptic operators, *Engineering Analysis with Boundary Elements* 31 (2007), 373–385.

[26] L. Marin, A meshless method for solving the Cauchy problem in three-dimensional elastostatics. *Computers & Mathematics with Applications* 50 (2005), 73–92.

[27] L. Marin and D. Lesnic, The method of fundamental solutions for the Cauchy problem in two-dimensional linear elasticity, *International Journal of Solids and Structures* 41 (2004), 3425–3438.

[28] L. Marin, Numerical solution of the Cauchy problem for steady-state heat transfer in two-dimensional functionally graded materials, *International Journal of Solids and Structures* 42 (2005), 4338–4351.

[29] B. T. Jin Y. Zheng, A meshless method for some inverse problems associated with the Helmholtz equation, *Computer Methods in Applied Mechanics and Engineering* 195 (2006), 2270–2280.

[30] L. Marin, A meshless method for the numerical solution of the Cauchy problem associated with three-dimensional Helmholtz-type equations, *Applied Mathematics and Computation* 165 (2005), 355–374.

[31] L. Marin and D. Lesnic, The method of fundamental solutions for the Cauchy problem associated with two-dimensional Helmholtz-type equations, *Computers & Structures* 83 (2005), 267–278.

[32] C. W. Chen, D. L. Young, C. C. Tsai, and K. Murugesan, The method of fundamental solutions for inverse 2D Stokes problems, *Computational Mechanics* 37 (2005), 2–14.

[33] L. Marin and D. Lesnic, The method of fundamental solutions for inverse boundary value problems associated with the two-dimensional biharmonic equation, *Mathematical and Computer Modelling* 42 (2005), 261–278.

[34] L. Marin and A. Karageorghis, The MFS for the Cauchy problem in two-dimensional steady-state linear thermoelasticity, *International Journal of Solids and Structures* 50 (2013), 3387–3398.

[35] A. Karageorghis, D. Lesnic, and L. Marin, The method of fundamental solutions for an inverse boundary value problem in static thermo-elasticity, *Computers & Structures* 135 (2014), 32–39.

[36] A. N. Tikhonov and V. Y. Arsenin, *Methods for Solving Ill-Posed Problems*. Nauka, Moscow, 1986.

[37] P. C. Hansen, *Rank-Deficient and Discrete Ill-Posed Problems: Numerical Aspects of Linear Inversion*. SIAM, Philadelphia, 1998.

[38] V. A. Morozov, On the solution of functional equations by the method of regularization, *Soviet Mathematics Doklady* 7 (1966), 414–417.

[39] G. H. Golub, M. Heath, G. Wahba, Generalized cross-validation as a method for choosing a good ridge parameter, *Technometrics* 22 (1979), 1–35.

[40] P. C. Hansen and D. P. O'Leary, The use of the L-curve in the regularization of discrete ill-posed problems, *SIAM Journal of Scientific Computing* 14 (1993), 1487–503.

[41] M. H. Aliabadi, *The Boundary Element Method. Applications in Solids and Structures. Volume 2.* John Wiley & Sons, London, 2002.

[42] P. Gorzelańczyk and J. A. Kołodziej, Some remarks concerning the shape of the shape contour with application of the method of fundamental solutions to elastic torsion of prismatic rods, *Engineering Analysis with Boundary Elements* 32 (2008), 64–75.

[43] P. C. Hansen, Regularization tools: a Matlab package for analysis and solution of discrete ill-posed problems, *Numerical Algorithms* 6 (1994), 1–35.

[44] P. C. Hansen, Regularization tools version 4.0 for Matlab 7.3, *Numerical Algorithms* 46 (2007), 189–194, available at www.netlib.org/numeralgo.

Figure Captions

Figure 1: The analytical and numerical (a) temperatures $\mathrm{T}\big|_{\Gamma_2}$, (b) normal heat fluxes $\mathrm{q}\big|_{\partial\Omega}$, and displacements (c) $\mathrm{u}_1\big|_{\Gamma_2}$ and (d) $\mathrm{u}_2\big|_{\Gamma_2}$, obtained using the TRM–LC approach and various levels of noise in $\mathrm{T}\big|_{\Gamma_1}$, $\mathbf{u}\big|_{\Gamma_1}$ and $\mathbf{t}\big|_{\Gamma_1}$, for Example 1 with $\theta_0 = \pi$.

Figure 2: The analytical and numerical (a) temperatures $\mathrm{T}\big|_{\Gamma_2}$, (b) normal heat fluxes $\mathrm{q}\big|_{\partial\Omega}$, and displacements (c) $\mathrm{u}_1\big|_{\Gamma_2}$ and (d) $\mathrm{u}_2\big|_{\Gamma_2}$, obtained using the DSVD–LC approach and various levels of noise in $\mathrm{T}\big|_{\Gamma_1}$, $\mathbf{u}\big|_{\Gamma_1}$ and $\mathbf{t}\big|_{\Gamma_1}$, for Example 1 with $\theta_0 = \pi$.

Figure 3: The analytical and numerical (a) temperatures $\mathrm{T}\big|_{\Gamma_2}$, (b) normal heat fluxes $\mathrm{q}\big|_{\partial\Omega}$, and displacements (c) $\mathrm{u}_1\big|_{\Gamma_2}$ and (d) $\mathrm{u}_2\big|_{\Gamma_2}$, obtained using the TSVD–DP approach and various levels of noise in $\mathrm{T}\big|_{\Gamma_1}$, $\mathbf{u}\big|_{\Gamma_1}$ and $\mathbf{t}\big|_{\Gamma_1}$, for Example 1 with $\theta_0 = \pi$.

Figure 4: The analytical and numerical (a) temperatures $\mathrm{T}\big|_{\Gamma_2}$, (b) normal heat fluxes $\mathrm{q}\big|_{\partial\Omega}$, and displacements (c) $\mathrm{u}_1\big|_{\Gamma_2}$ and (d) $\mathrm{u}_2\big|_{\Gamma_2}$, obtained using the TRM–LC approach and various levels of noise in $\mathrm{T}\big|_{\Gamma_1}$, $\mathbf{u}\big|_{\Gamma_1}$ and $\mathbf{t}\big|_{\Gamma_1}$, for Example 1 with $\theta_0 = 4\pi/3$.

Figure 5: The analytical and numerical (a) temperatures $\mathrm{T}\big|_{\Gamma_2}$, (b) normal heat fluxes $\mathrm{q}\big|_{\partial\Omega}$, and displacements (c) $\mathrm{u}_1\big|_{\Gamma_2}$ and (d) $\mathrm{u}_2\big|_{\Gamma_2}$, obtained using the DSVD–LC approach and various levels of noise in $\mathrm{T}\big|_{\Gamma_1}$, $\mathbf{u}\big|_{\Gamma_1}$ and $\mathbf{t}\big|_{\Gamma_1}$, for Example 1 with $\theta_0 = 4\pi/3$.

Figure 6: The analytical and numerical (a) temperatures $\mathrm{T}\big|_{\Gamma_2}$, (b) normal heat fluxes $\mathrm{q}\big|_{\partial\Omega}$, and displacements (c) $\mathrm{u}_1\big|_{\Gamma_2}$ and (d) $\mathrm{u}_2\big|_{\Gamma_2}$, obtained using the TSVD–DP approach and various levels of noise in $\mathrm{T}\big|_{\Gamma_1}$, $\mathbf{u}\big|_{\Gamma_1}$ and $\mathbf{t}\big|_{\Gamma_1}$, for Example 1 with $\theta_0 = 4\pi/3$.

Figure 7: The analytical and numerical (a) temperatures $\mathrm{T}\big|_{\Gamma_2}$, (b) normal heat fluxes $\mathrm{q}\big|_{\partial\Omega}$, and displacements (c) $\mathrm{u}_1\big|_{\Gamma_2}$ and (d) $\mathrm{u}_2\big|_{\Gamma_2}$, obtained using the TRM–LC approach and various levels of noise in $\mathrm{T}\big|_{\Gamma_1}$, $\mathbf{u}\big|_{\Gamma_1}$ and $\mathbf{t}\big|_{\Gamma_1}$, for Example 1 with $\theta_0 = 2\pi/3$.

Figure 8: The analytical and numerical (a) temperatures $\mathrm{T}\big|_{\Gamma_2}$, (b) normal heat fluxes $\mathrm{q}\big|_{\partial\Omega}$, and displacements (c) $\mathrm{u}_1\big|_{\Gamma_2}$ and (d) $\mathrm{u}_2\big|_{\Gamma_2}$, obtained using the DSVD–LC approach and various levels of noise in $\mathrm{T}\big|_{\Gamma_1}$, $\mathbf{u}\big|_{\Gamma_1}$ and $\mathbf{t}\big|_{\Gamma_1}$, for Example 1 with $\theta_0 = 2\pi/3$.

Figure 9: The analytical and numerical (a) temperatures $\mathrm{T}\big|_{\Gamma_2}$, (b) normal heat fluxes $\mathrm{q}\big|_{\partial\Omega}$, and displacements (c) $\mathrm{u}_1\big|_{\Gamma_2}$ and (d) $\mathrm{u}_2\big|_{\Gamma_2}$, obtained using the TSVD–DP approach and various levels of noise in $\mathrm{T}\big|_{\Gamma_1}$, $\mathbf{u}\big|_{\Gamma_1}$ and $\mathbf{t}\big|_{\Gamma_1}$, for Example 1 with $\theta_0 = 2\pi/3$.

Figure 10: The analytical and numerical (a) temperatures $\mathrm{T}\big|_{\Gamma_2}$, (b) normal heat fluxes $\mathrm{q}\big|_{\Gamma_2}$, displacements (c) $\mathrm{u}_1\big|_{\Gamma_2}$, and tractions (d) $\mathrm{t}_2\big|_{\Gamma_2}$, obtained using the TRM–LC approach and various levels of noise in $\mathrm{T}\big|_{\Gamma_1}$ and $\mathbf{u}\big|_{\Gamma_1}$, for Example 2.

Figure 11: The analytical and numerical (a) temperatures $\mathrm{T}\big|_{\Gamma_2}$, (b) normal heat fluxes $\mathrm{q}\big|_{\Gamma_2}$, displacements (c) $\mathrm{u}_1\big|_{\Gamma_2}$, and tractions (d) $\mathrm{t}_2\big|_{\Gamma_2}$, obtained using the DSVD–LC approach and various levels of noise in $\mathrm{T}\big|_{\Gamma_1}$ and $\mathbf{u}\big|_{\Gamma_1}$, for Example 2.

Figure 12: The analytical and numerical (a) temperatures $\mathrm{T}\big|_{\Gamma_2}$, (b) normal heat fluxes $\mathrm{q}\big|_{\Gamma_2}$, displacements (c) $\mathrm{u}_1\big|_{\Gamma_2}$, and tractions (d) $\mathrm{t}_2\big|_{\Gamma_2}$, obtained using the TSVD–DP approach and various levels of noise in $\mathrm{T}\big|_{\Gamma_1}$ and $\mathbf{u}\big|_{\Gamma_1}$, for Example 2.

FIGURE 13: The analytical and numerical (a) temperatures $T\big|_{\Gamma_2}$, (b) normal heat fluxes $q\big|_{\Gamma_2}$, and displacements (c) $u_1\big|_{\Gamma_2}$ and (d) $u_2\big|_{\Gamma_2}$, obtained using the TRM–LC approach and various levels of noise in $\mathbf{u}\big|_{\Gamma_1}$ and $\mathbf{t}\big|_{\Gamma_1}$, for Example 3.

FIGURE 14: The analytical and numerical (a) temperatures $T\big|_{\Gamma_2}$, (b) normal heat fluxes $q\big|_{\Gamma_2}$, and displacements (c) $u_1\big|_{\Gamma_2}$ and (d) $u_2\big|_{\Gamma_2}$, obtained using the DSVD–LC approach and various levels of noise in $\mathbf{u}\big|_{\Gamma_1}$ and $\mathbf{t}\big|_{\Gamma_1}$, for Example 3.

FIGURE 15: The analytical and numerical (a) temperatures $T\big|_{\Gamma_2}$, (b) normal heat fluxes $q\big|_{\Gamma_2}$, and displacements (c) $u_1\big|_{\Gamma_2}$ and (d) $u_2\big|_{\Gamma_2}$, obtained using the TSVD–DP approach and various levels of noise in $\mathbf{u}\big|_{\Gamma_1}$ and $\mathbf{t}\big|_{\Gamma_1}$, for Example 3.

FIGURE 16: The RMS errors $e_{\Gamma_2}(T)$, $e_{\partial\Omega}(q)$ and $e_{\Gamma_2}(\mathbf{u})$ as functions of the distance d, obtained using (a) TRM–LC, (b) DSVD–LC and (c) TSVD–DP, for the inverse problem (B) given by Example 1 with $\theta_0 = \pi$ and $p_T = p_{\mathbf{u}} = p_{\mathbf{t}} = 1\%$ noise.

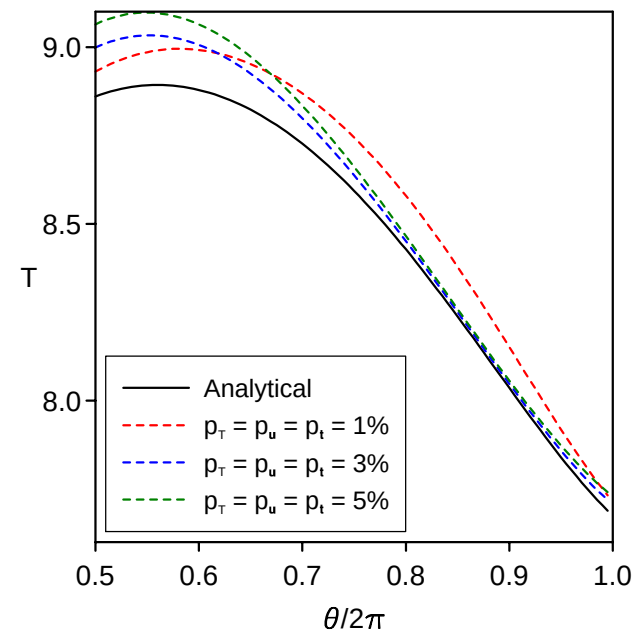

(a) Example 1: $\mathrm{T}\big|_{\Gamma_2}$

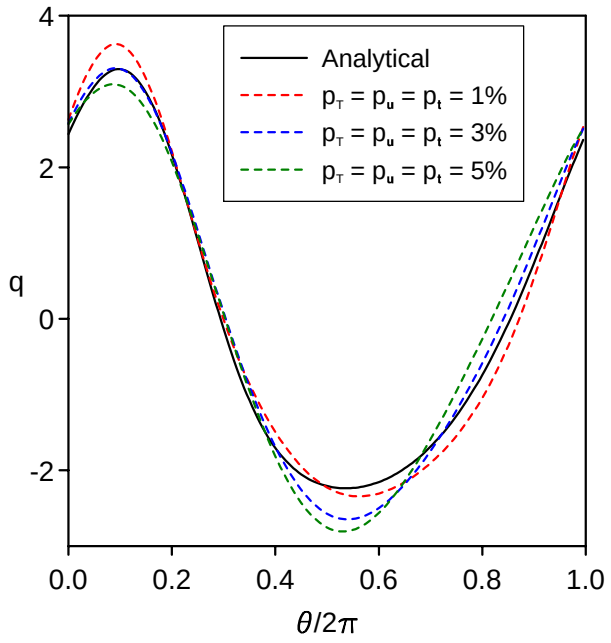

(b) Example 1: $\mathrm{q}\big|_{\partial\Omega}$

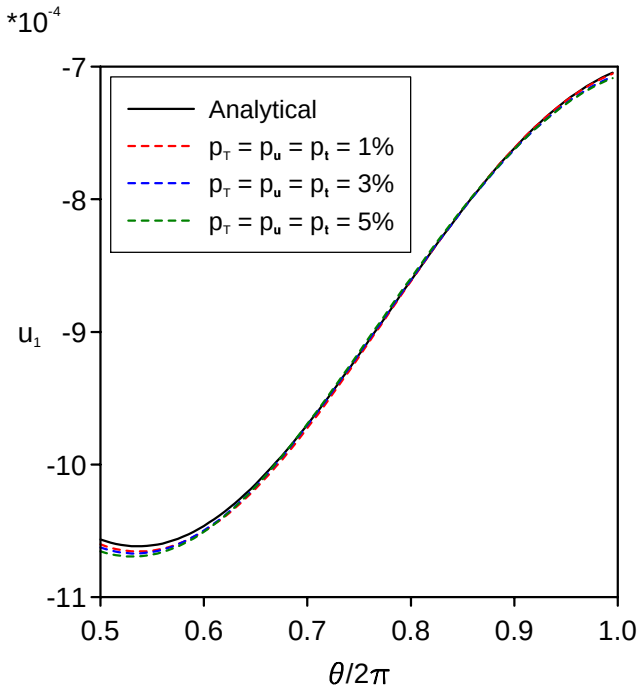

(c) Example 1: $\mathrm{u}_1\big|_{\Gamma_2}$

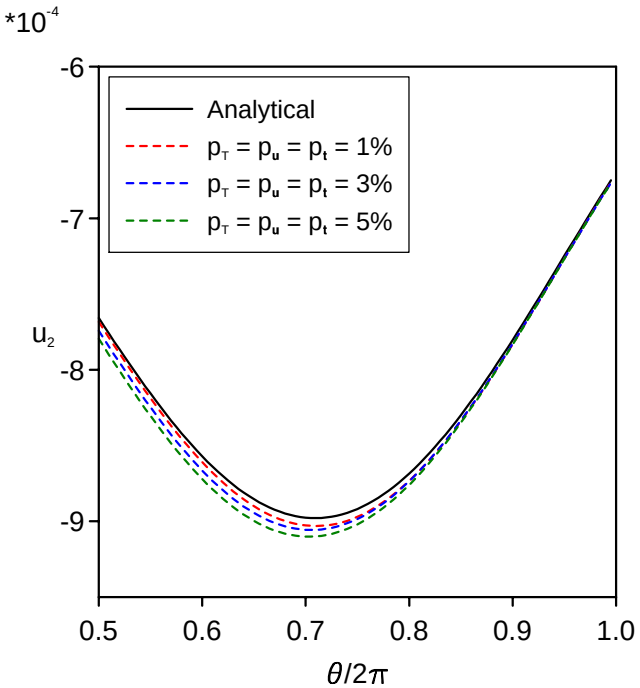

(d) Example 1: $\mathrm{u}_2\big|_{\Gamma_2}$

Figure 1:

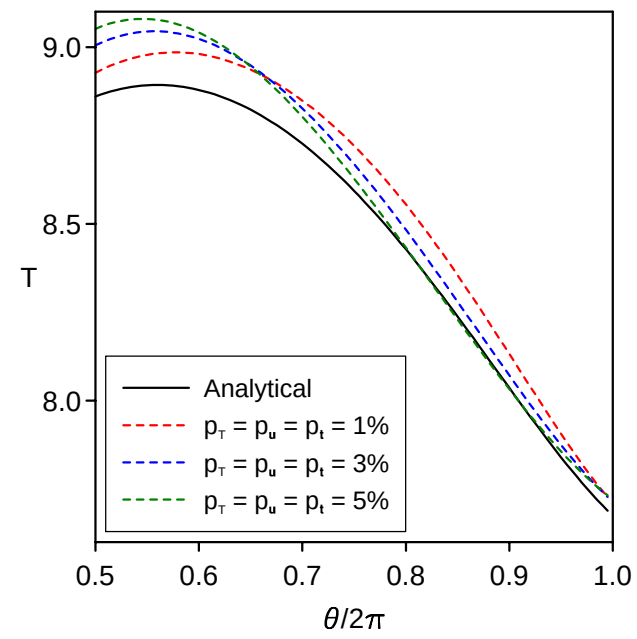

(a) Example 1: $\mathrm{T}|_{\Gamma_2}$

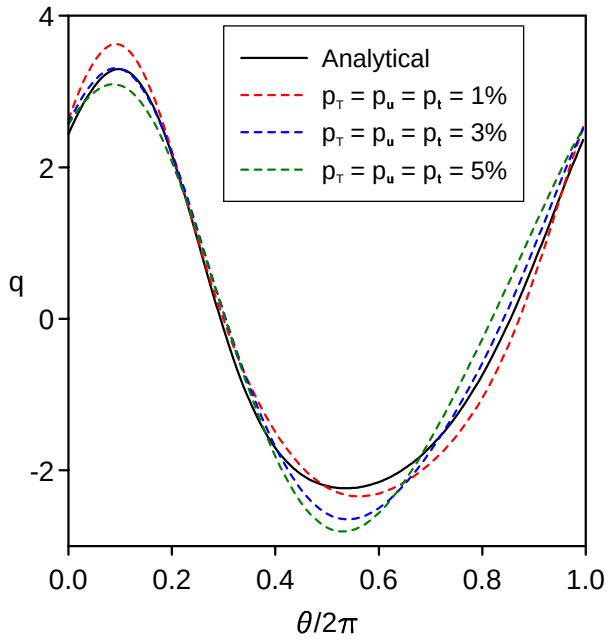

(b) Example 1: $\mathrm{q}|_{\partial\Omega}$

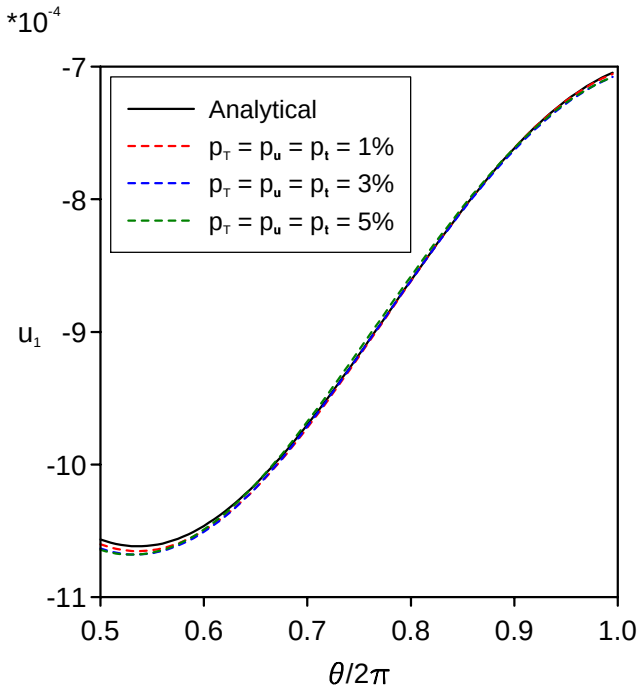

(c) Example 1: $\mathrm{u}_1|_{\Gamma_2}$

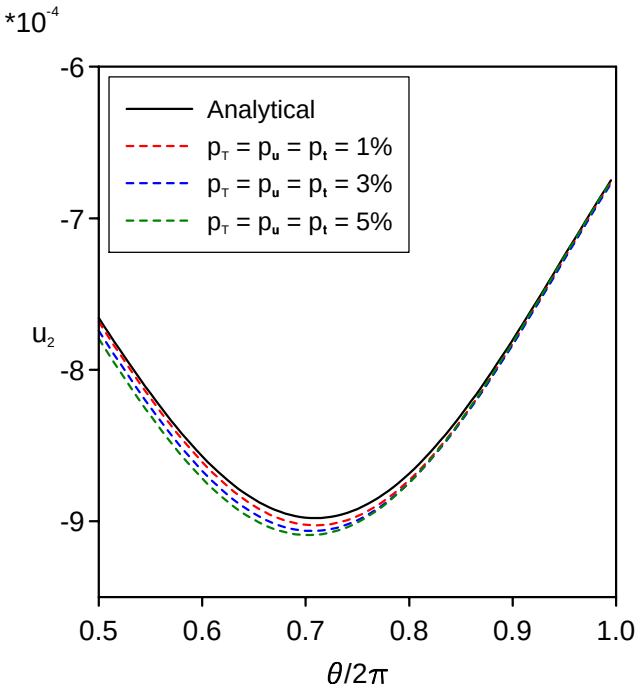

(d) Example 1: $\mathrm{u}_2|_{\Gamma_2}$

Figure 2:

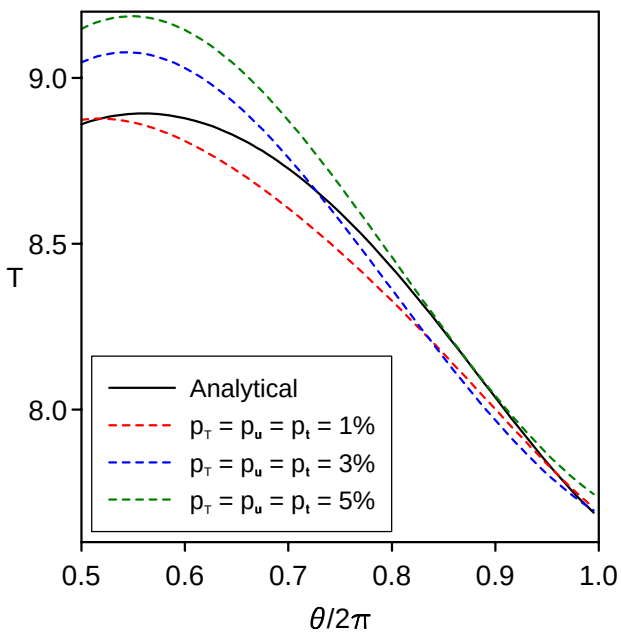

(a) Example 1: $\mathrm{T}|_{\Gamma_2}$

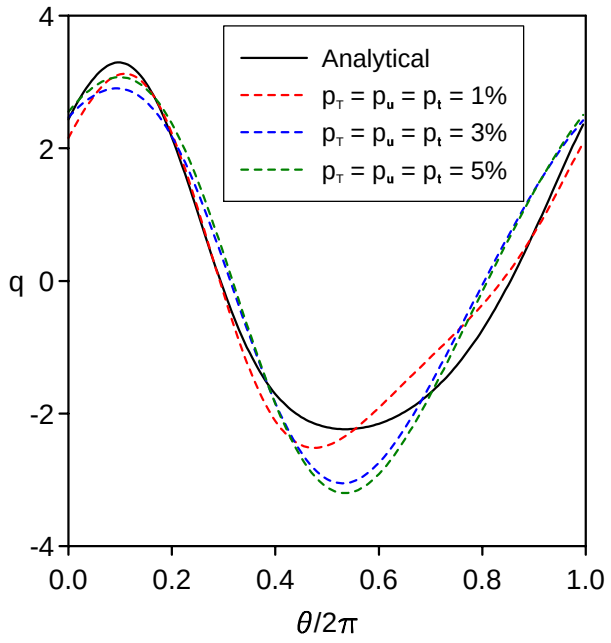

(b) Example 1: $\mathrm{q}|_{\partial\Omega}$

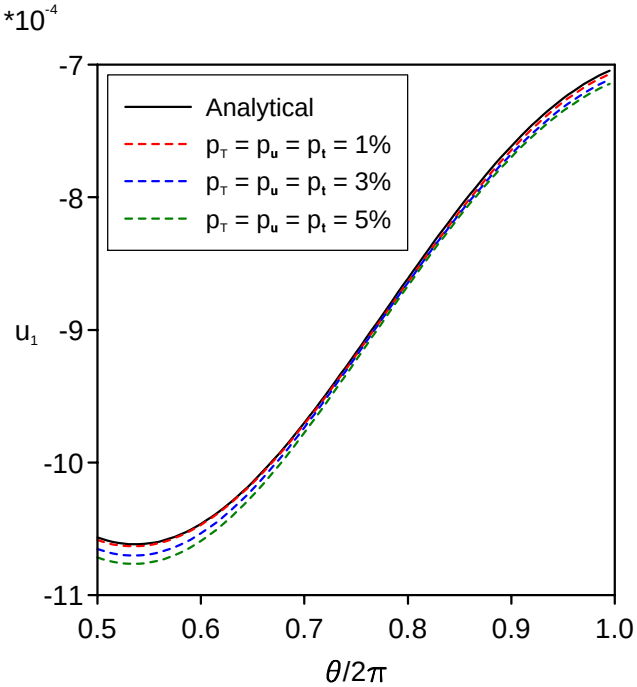

(c) Example 1: $\mathrm{u}_1|_{\Gamma_2}$

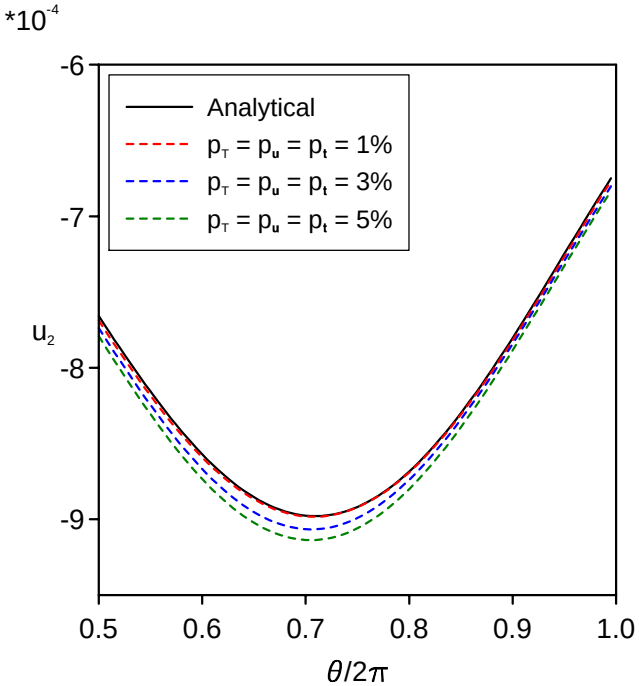

(d) Example 1: $\mathrm{u}_2|_{\Gamma_2}$

Figure 3:

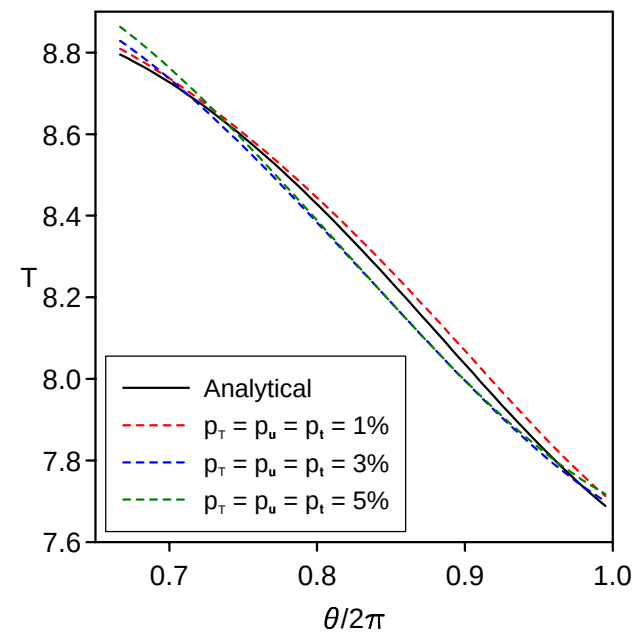

(a) Example 1: $\mathrm{T}\big|_{\Gamma_2}$

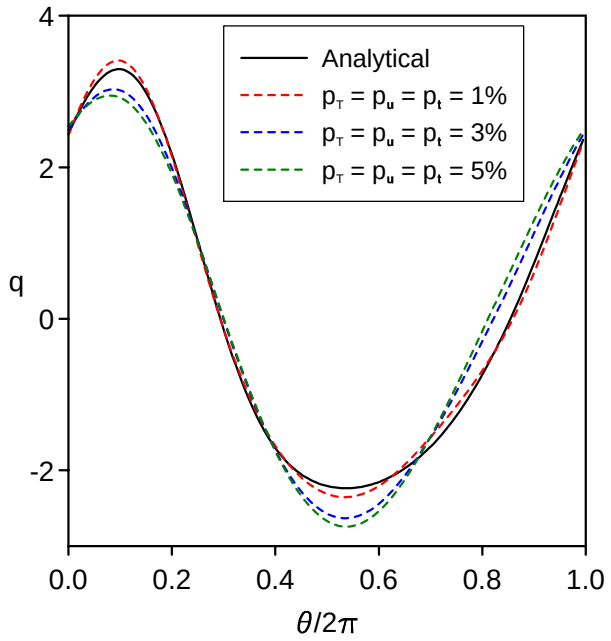

(b) Example 1: $\mathrm{q}\big|_{\partial\Omega}$

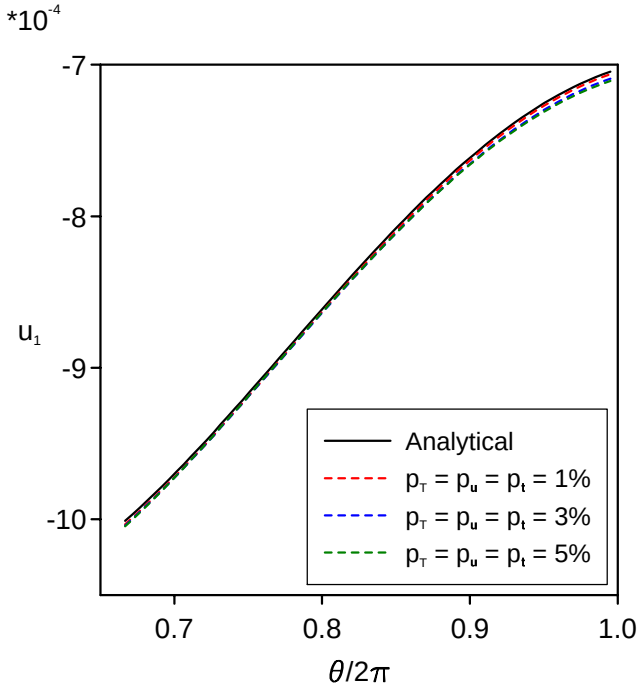

(c) Example 1: $\mathrm{u}_1\big|_{\Gamma_2}$

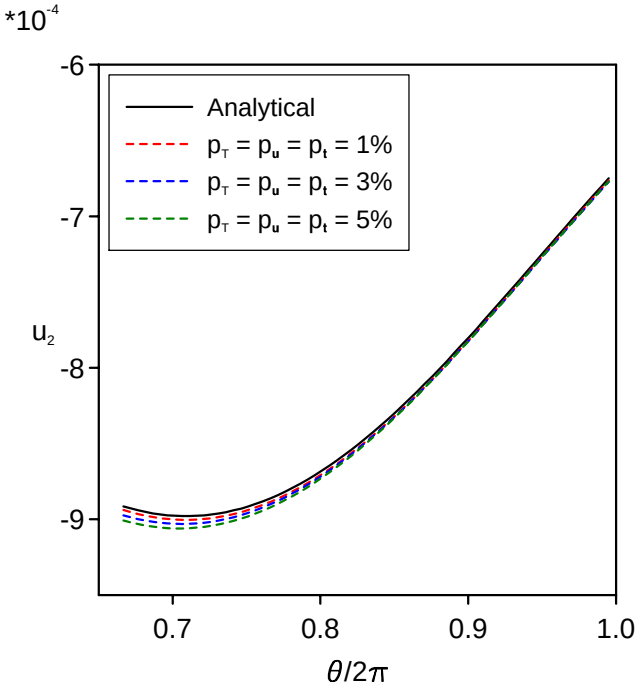

(d) Example 1: $\mathrm{u}_2\big|_{\Gamma_2}$

Figure 4:

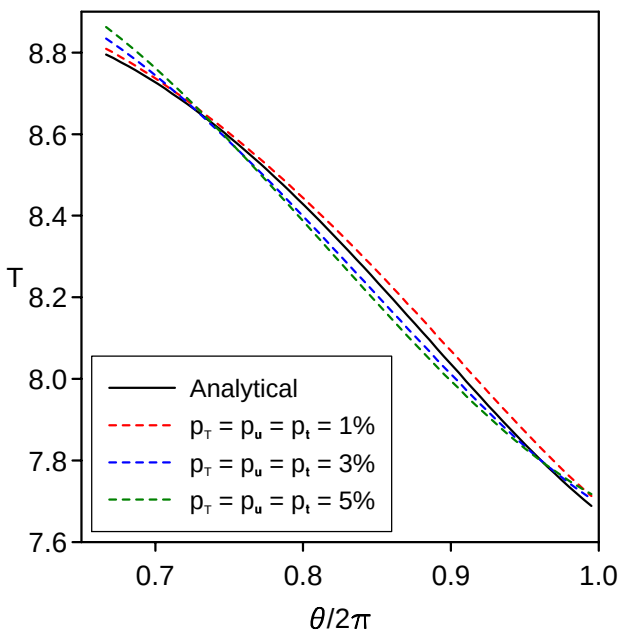

(a) Example 1: $\mathrm{T}|_{\Gamma_2}$

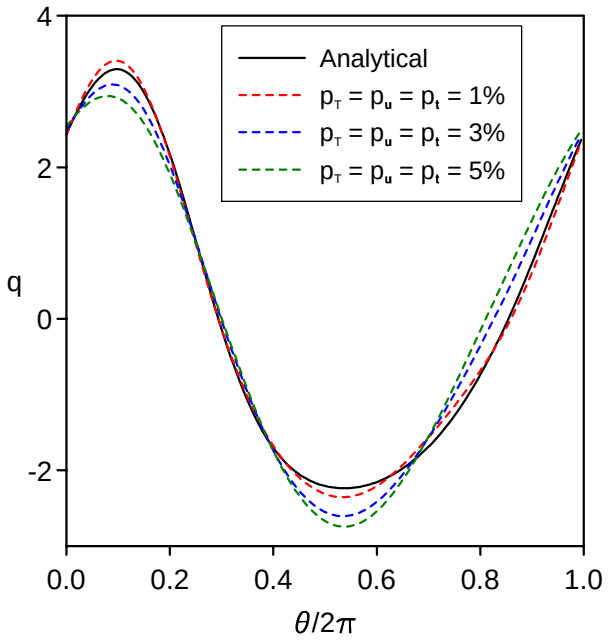

(b) Example 1: $\mathrm{q}|_{\partial\Omega}$

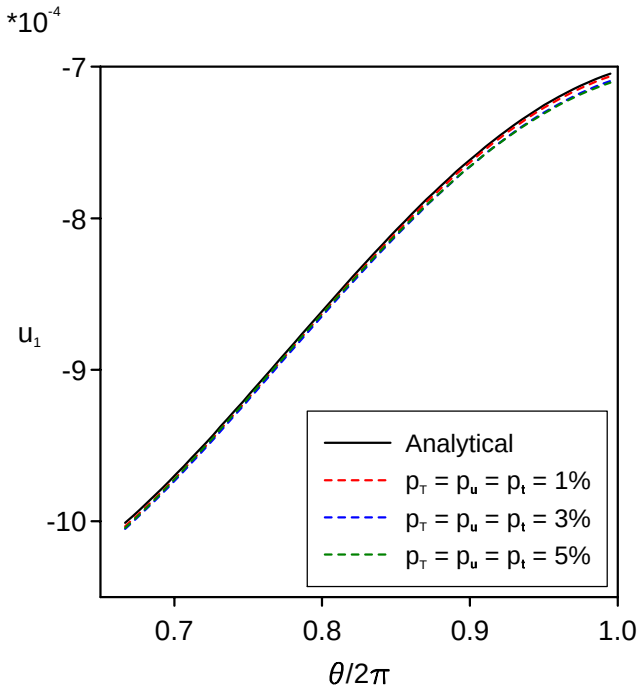

(c) Example 1: $\mathrm{u}_1|_{\Gamma_2}$

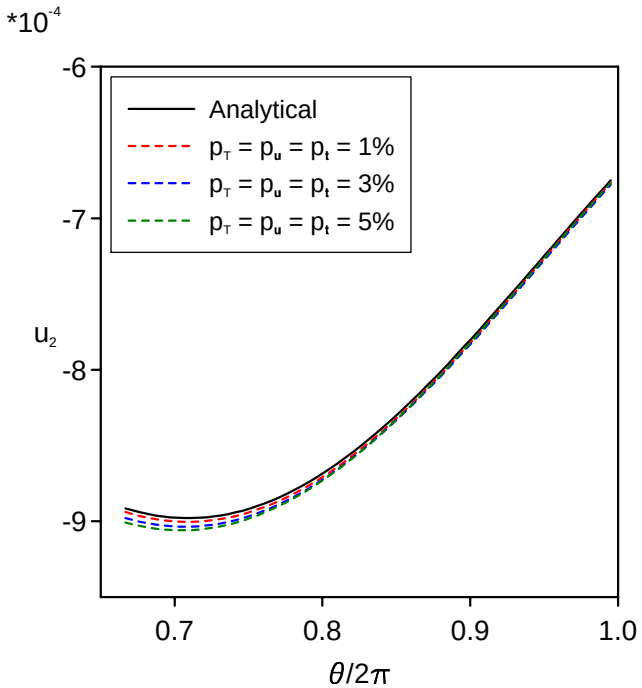

(d) Example 1: $\mathrm{u}_2|_{\Gamma_2}$

Figure 5:

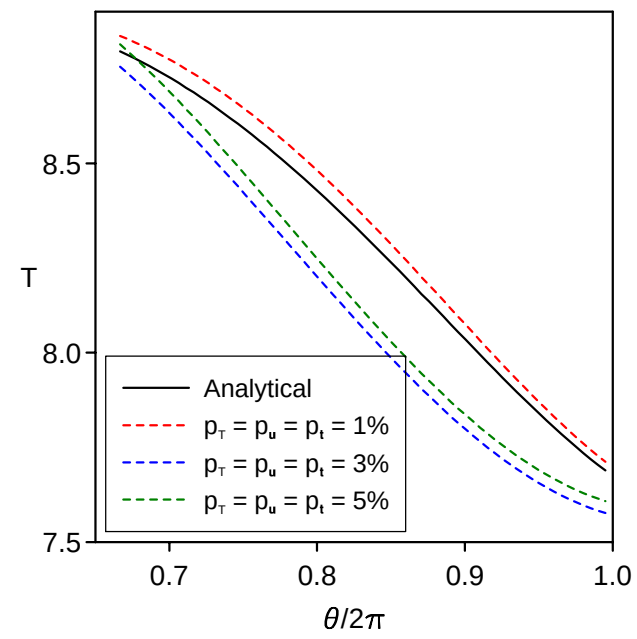

(a) Example 1: $\mathrm{T}\big|_{\Gamma_2}$

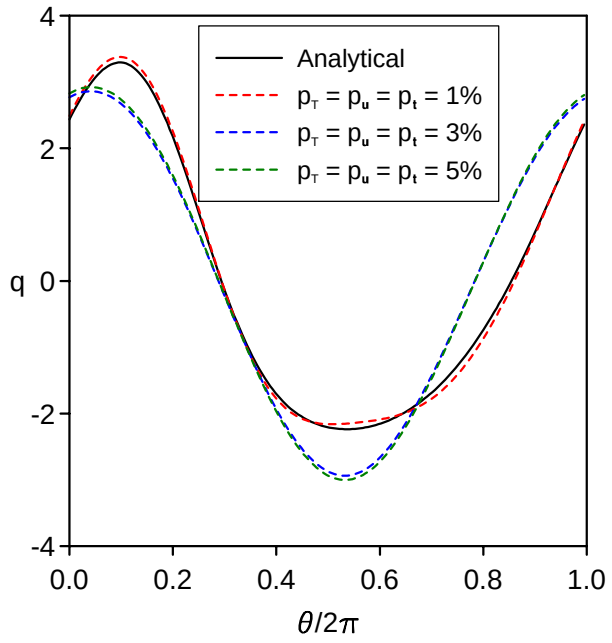

(b) Example 1: $\mathrm{q}\big|_{\partial\Omega}$

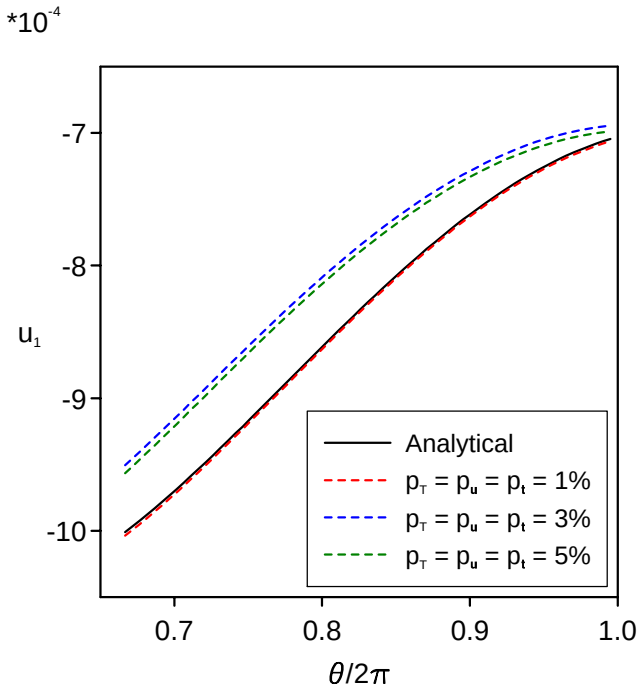

(c) Example 1: $\mathrm{u}_1\big|_{\Gamma_2}$

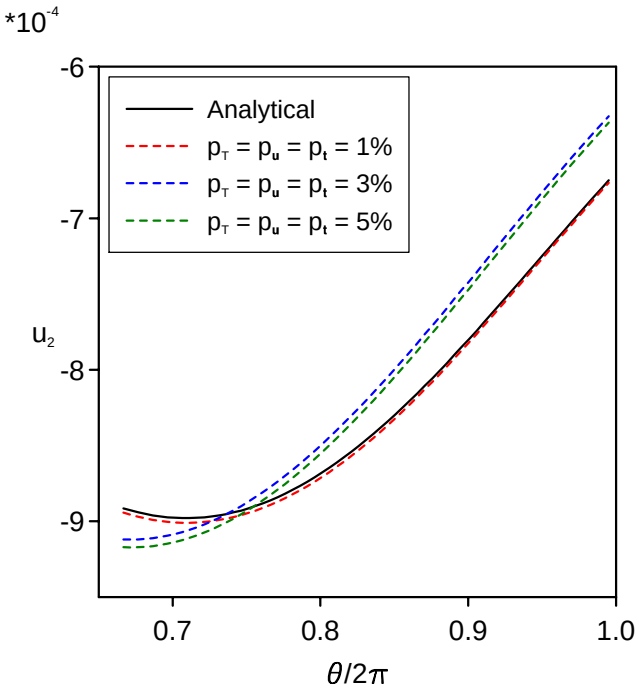

(d) Example 1: $\mathrm{u}_2\big|_{\Gamma_2}$

Figure 6:

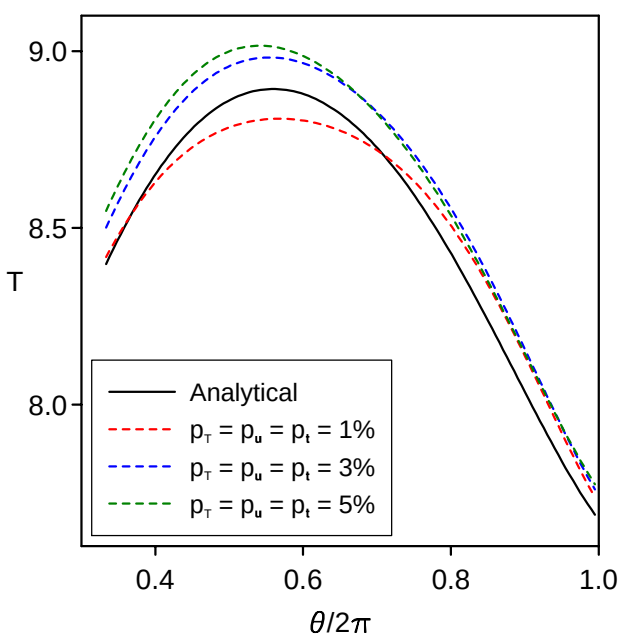

(a) Example 1: $\mathrm{T}\big|_{\Gamma_2}$

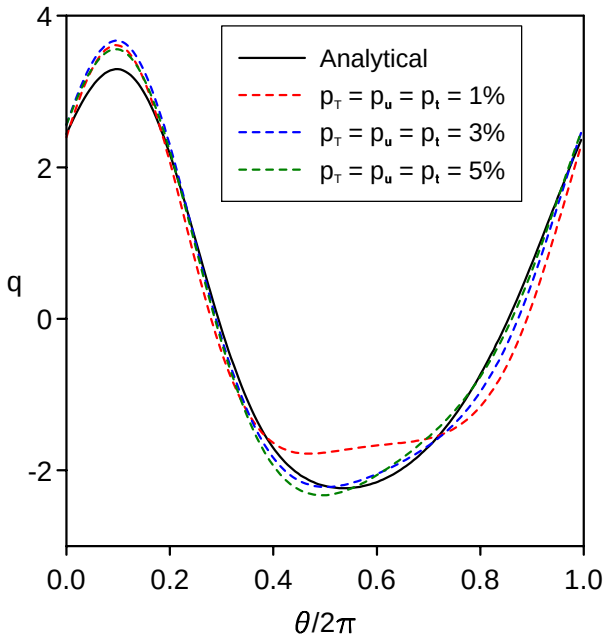

(b) Example 1: $\mathrm{q}\big|_{\partial\Omega}$

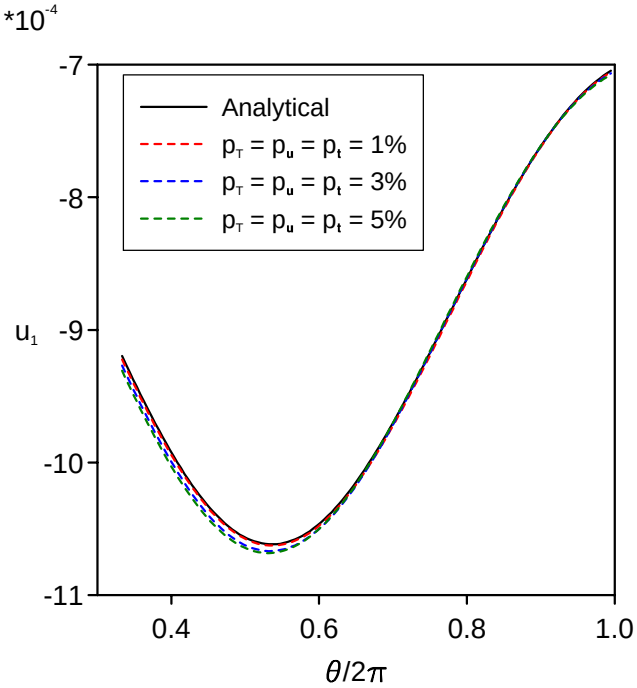

(c) Example 1: $\mathrm{u}_1\big|_{\Gamma_2}$

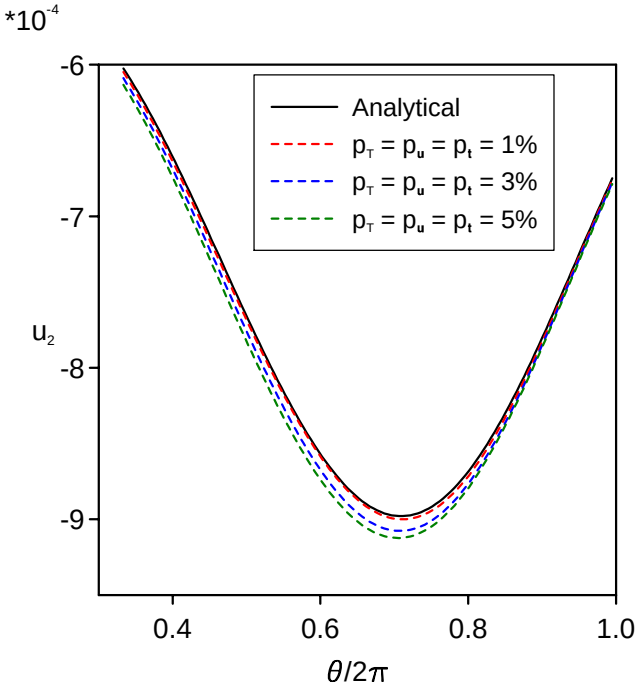

(d) Example 1: $\mathrm{u}_2\big|_{\Gamma_2}$

Figure 7:

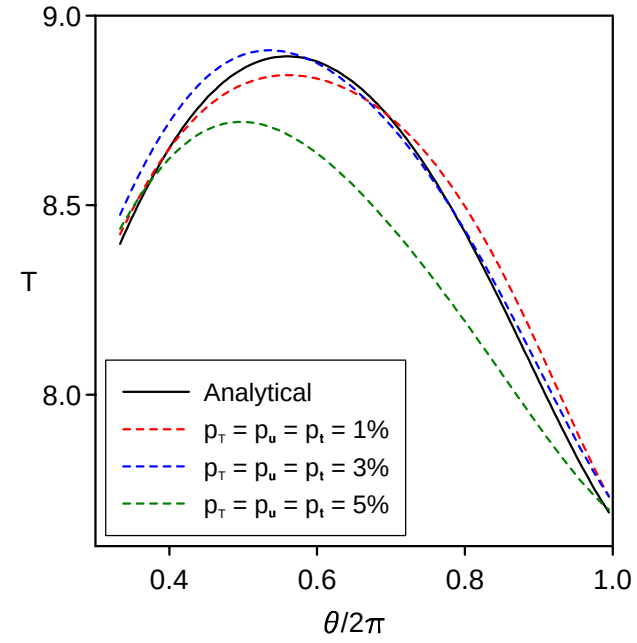

(a) Example 1: $\mathrm{T}|_{\Gamma_2}$

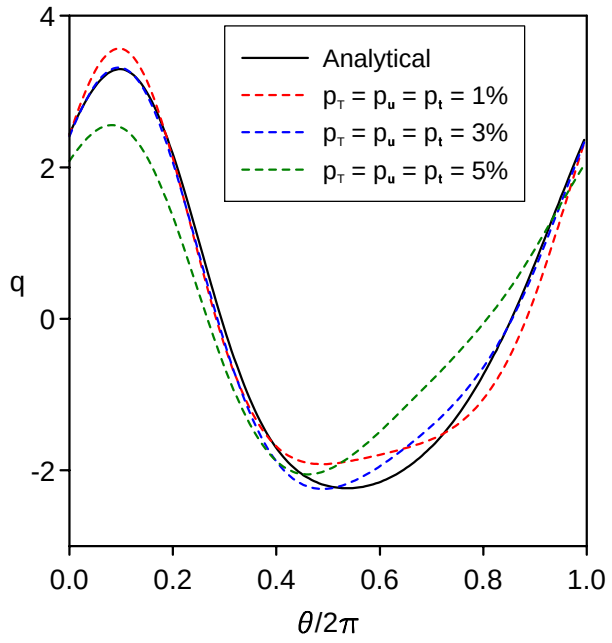

(b) Example 1: $\mathrm{q}|_{\partial\Omega}$

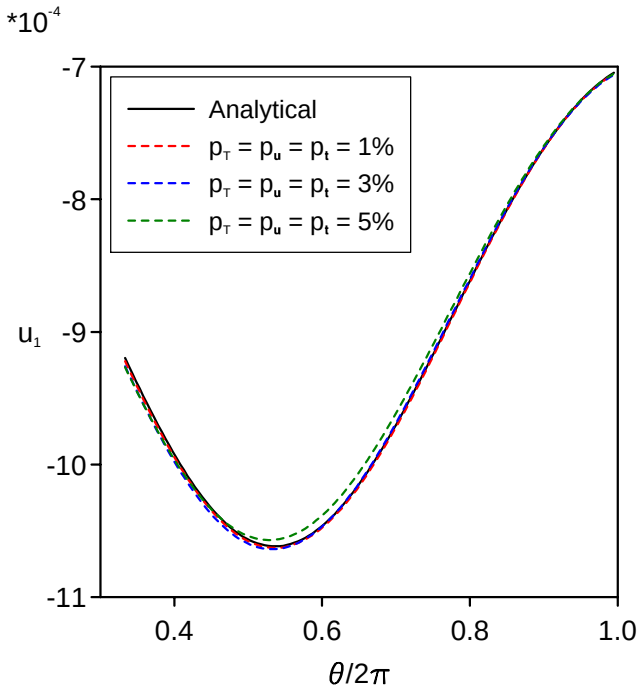

(c) Example 1: $\mathrm{u}_1|_{\Gamma_2}$

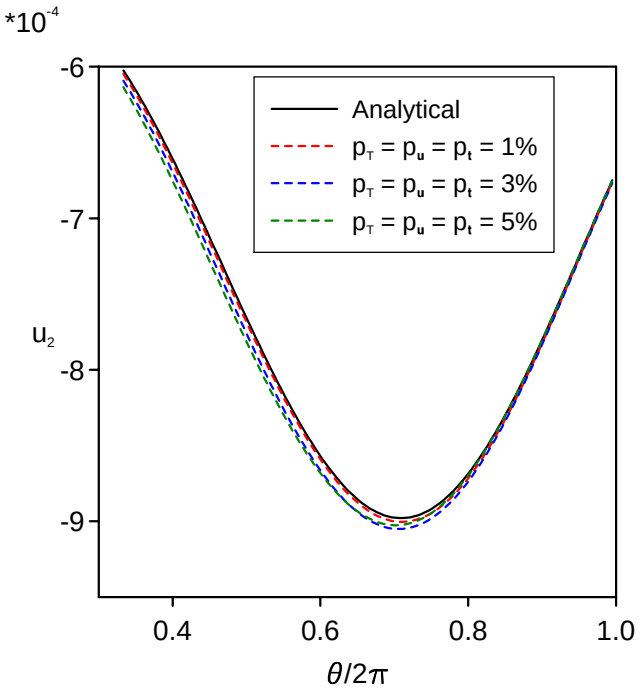

(d) Example 1: $\mathrm{u}_2|_{\Gamma_2}$

Figure 8:

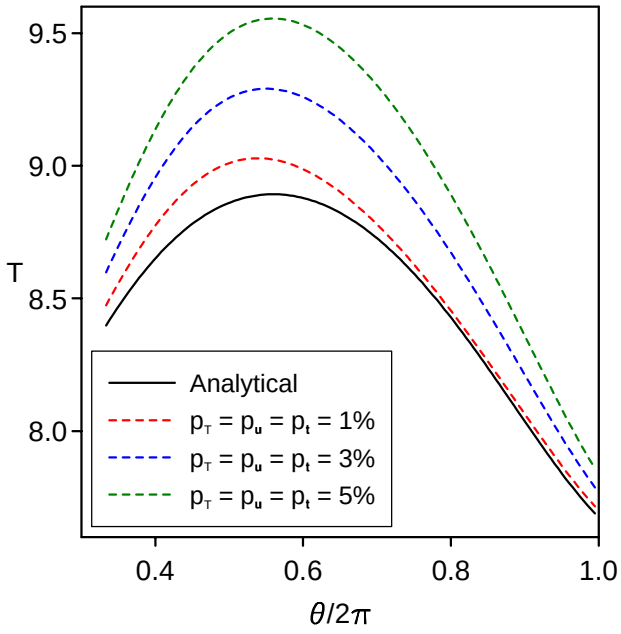

(a) Example 1: $\mathrm{T}\big|_{\Gamma_2}$

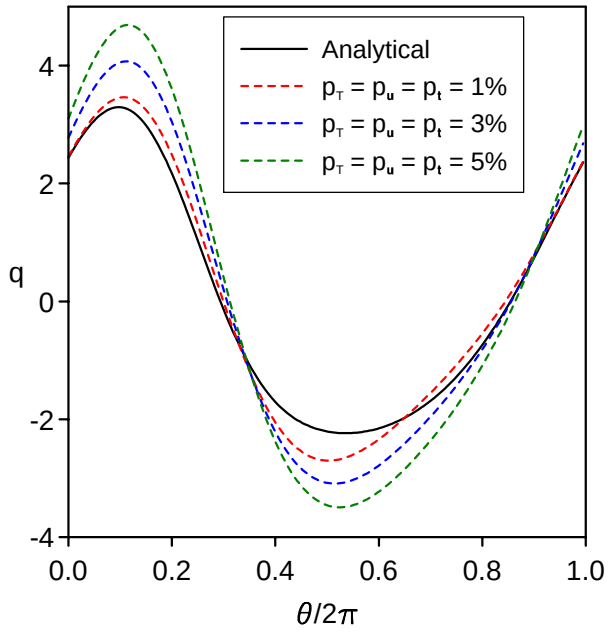

(b) Example 1: $\mathrm{q}\big|_{\partial\Omega}$

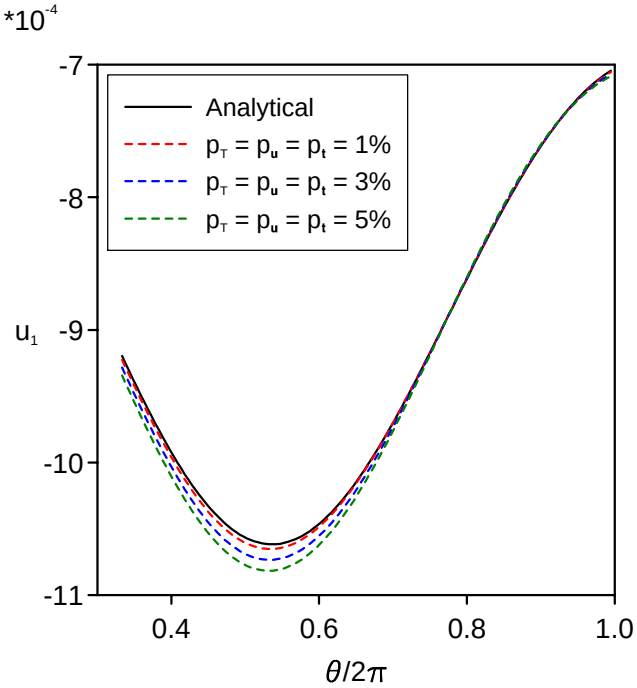

(c) Example 1: $\mathrm{u}_1\big|_{\Gamma_2}$

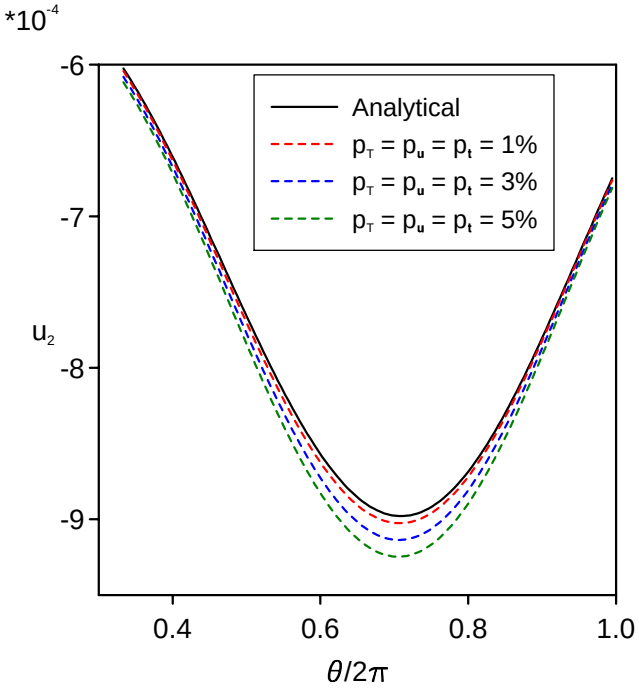

(d) Example 1: $\mathrm{u}_2\big|_{\Gamma_2}$

Figure 9:

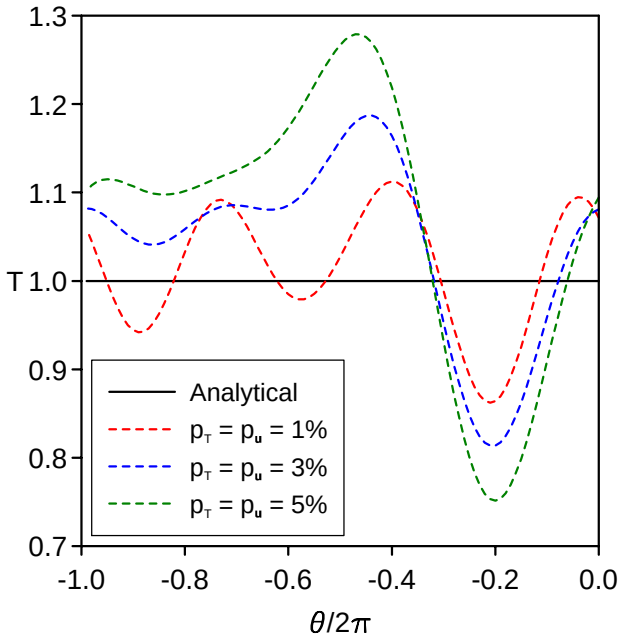

(a) Example 2: $\mathrm{T}|_{\Gamma_2}$

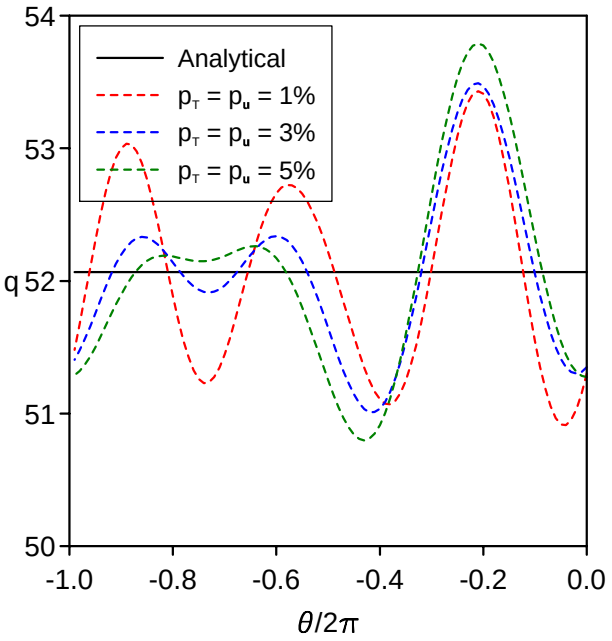

(b) Example 2: $\mathrm{q}|_{\Gamma_2}$

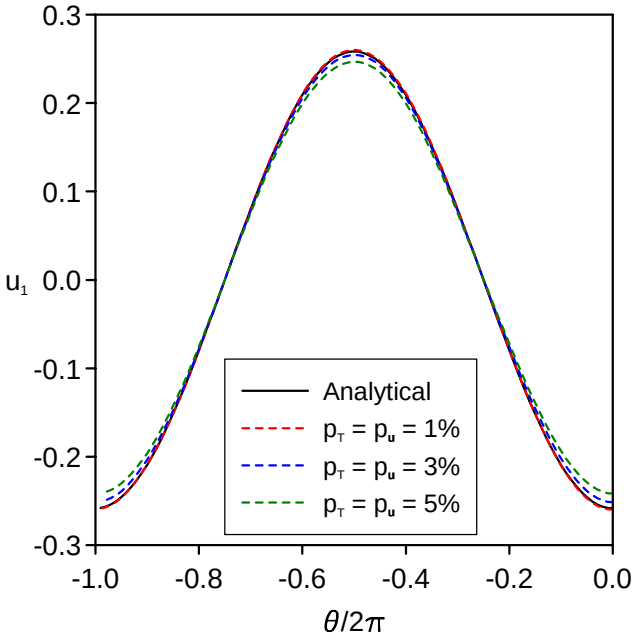

(c) Example 2: $\mathrm{u}_1|_{\Gamma_2}$

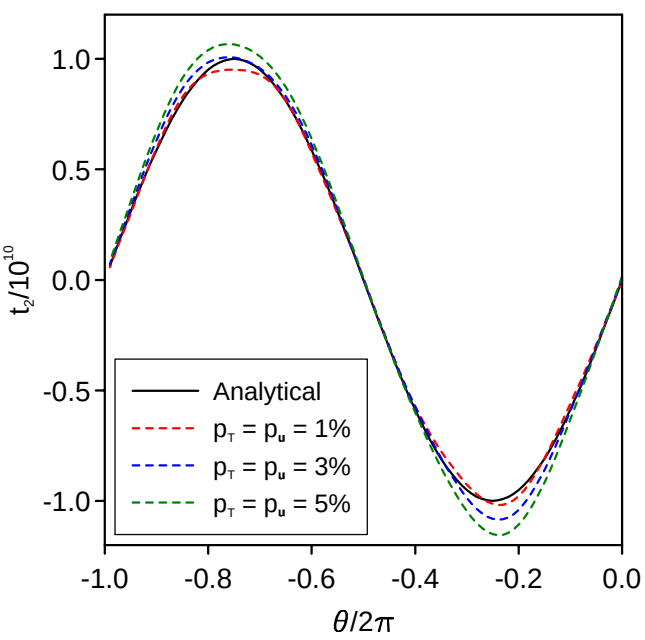

(d) Example 2: $\mathrm{t}_2|_{\Gamma_2}$

Figure 10:

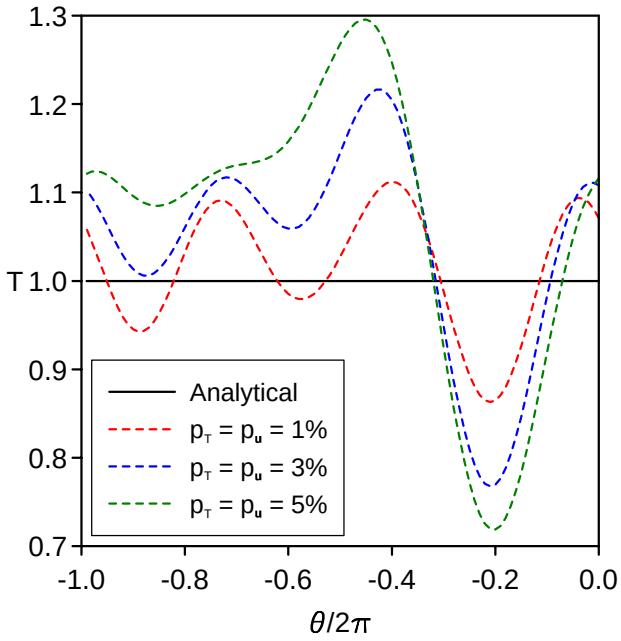

(a) Example 2: $\mathrm{T}|_{\Gamma_2}$

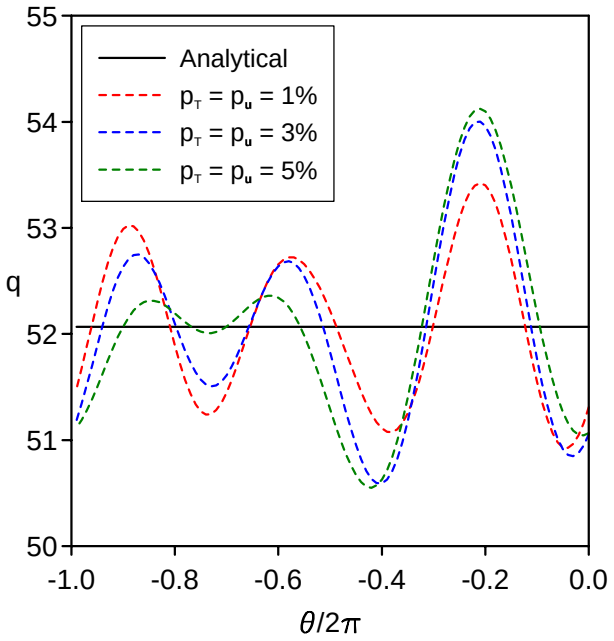

(b) Example 2: $\mathrm{q}|_{\Gamma_2}$

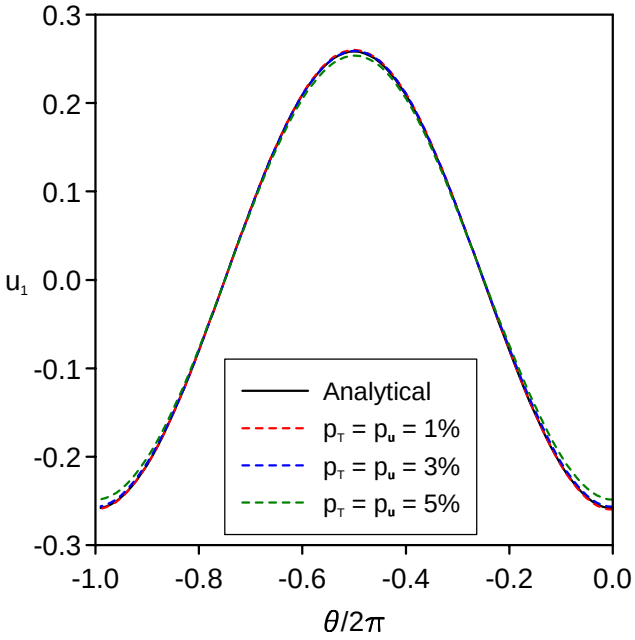

(c) Example 2: $\mathrm{u}_1|_{\Gamma_2}$

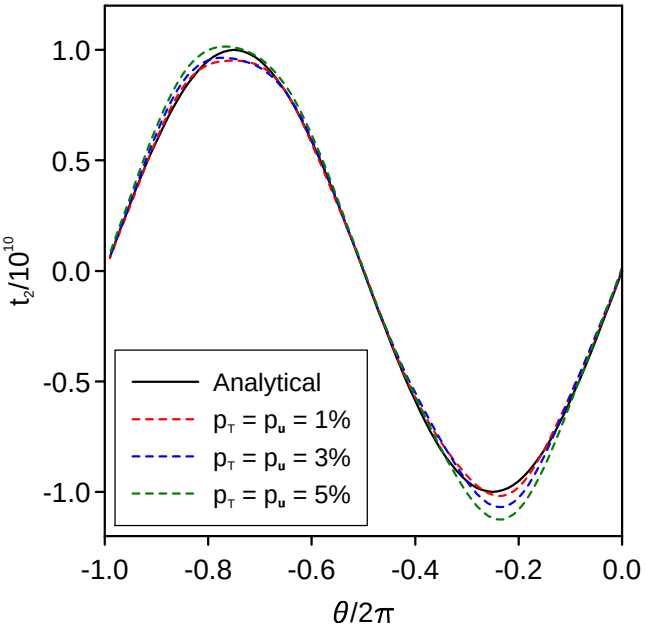

(d) Example 2: $\mathrm{u}_2|_{\Gamma_2}$

Figure 11:

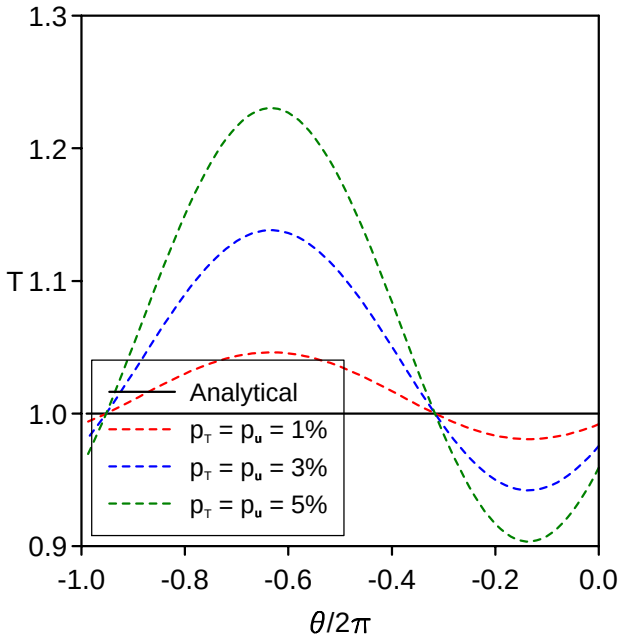

(a) Example 2: $\mathrm{T}|_{\Gamma_2}$

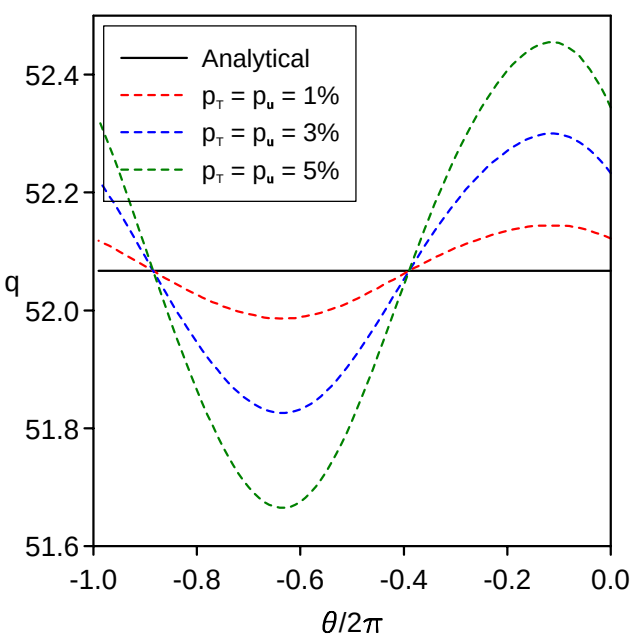

(b) Example 2: $\mathrm{q}|_{\Gamma_2}$

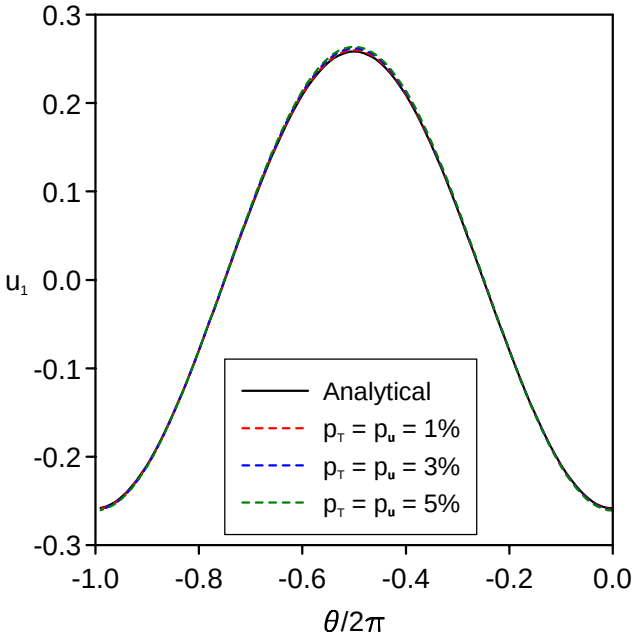

(c) Example 2: $\mathrm{u}_1|_{\Gamma_2}$

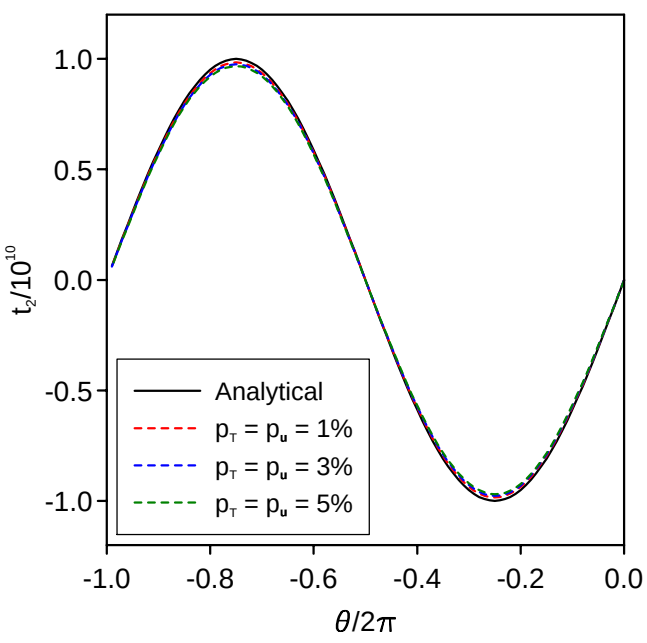

(d) Example 2: $\mathrm{u}_2|_{\Gamma_2}$

Figure 12:

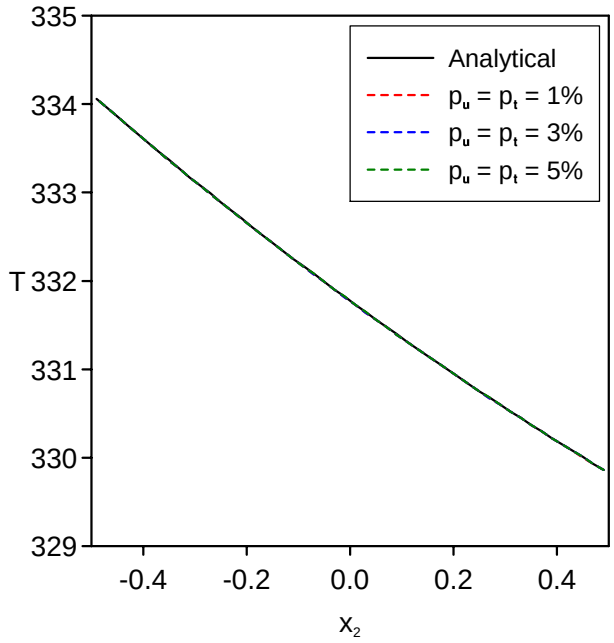

(a) Example 3: $T|_{\Gamma_2}$

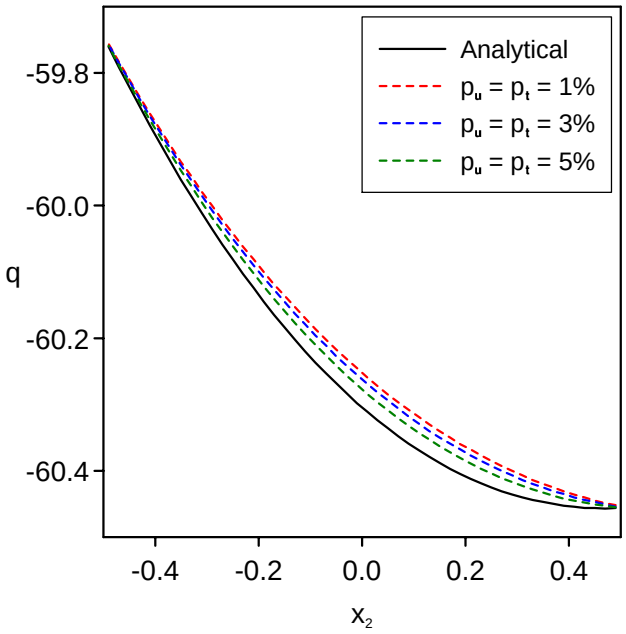

(b) Example 3: $q|_{\Gamma_2}$

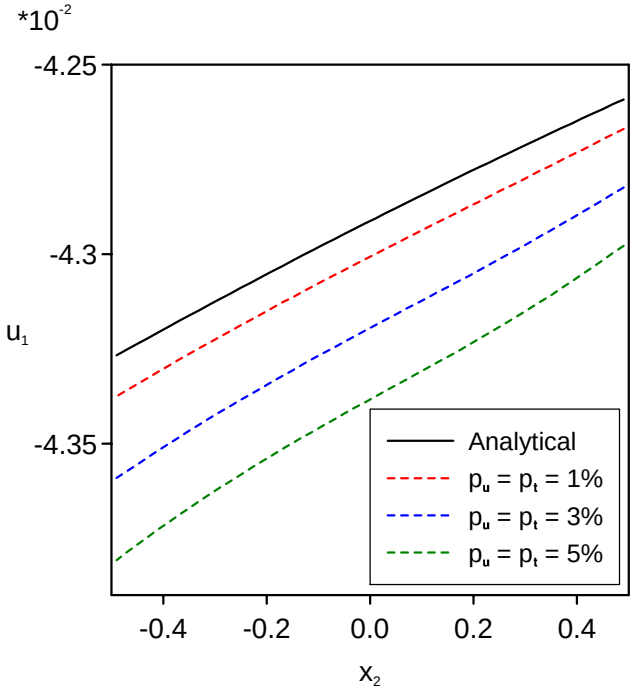

(c) Example 3: $u_1|_{\Gamma_2}$

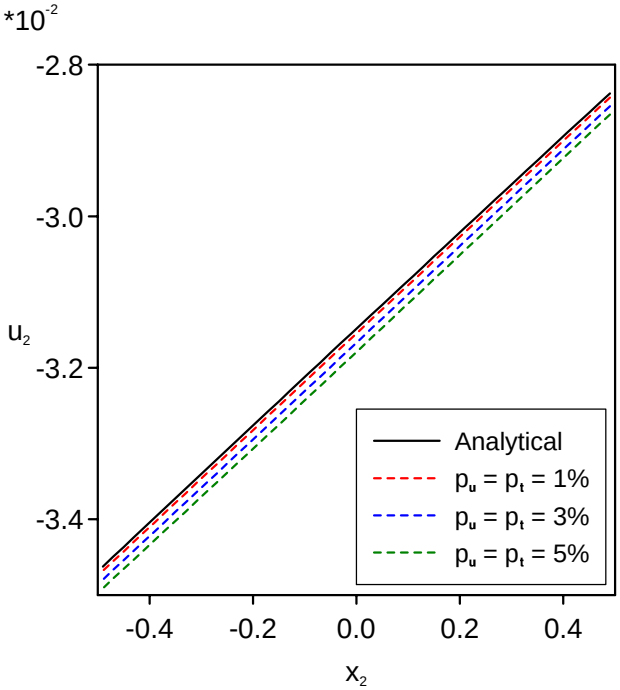

(d) Example 3: $t_2|_{\Gamma_2}$

Figure 13:

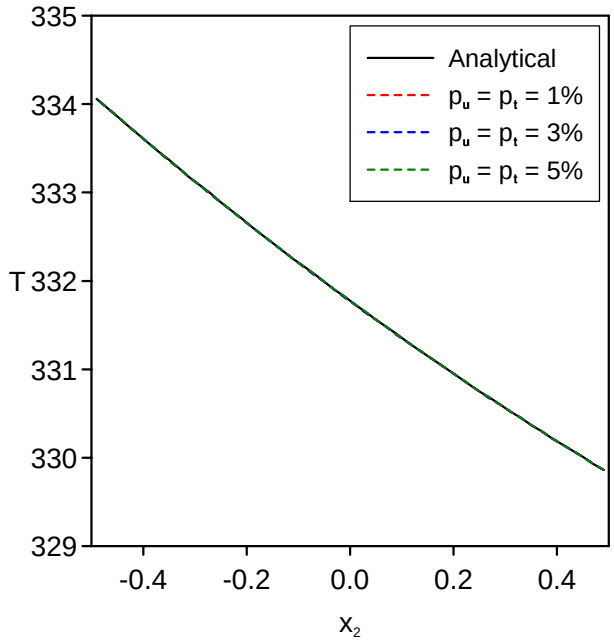

(a) Example 3: $T|_{\Gamma_2}$

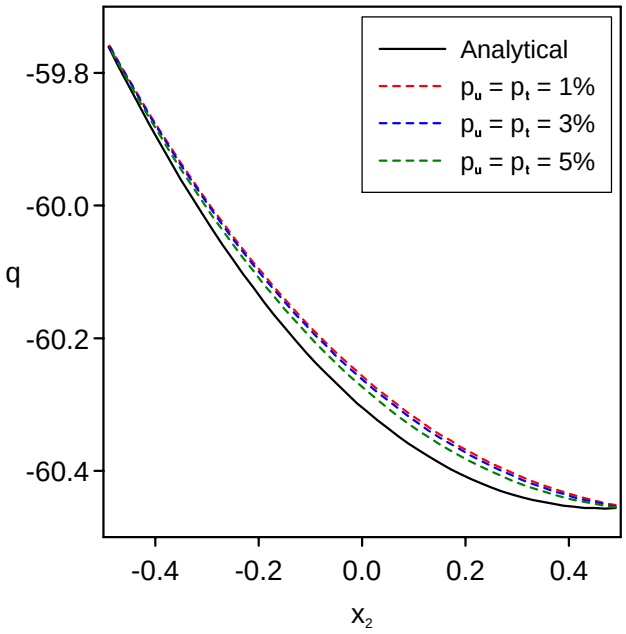

(b) Example 3: $q|_{\Gamma_2}$

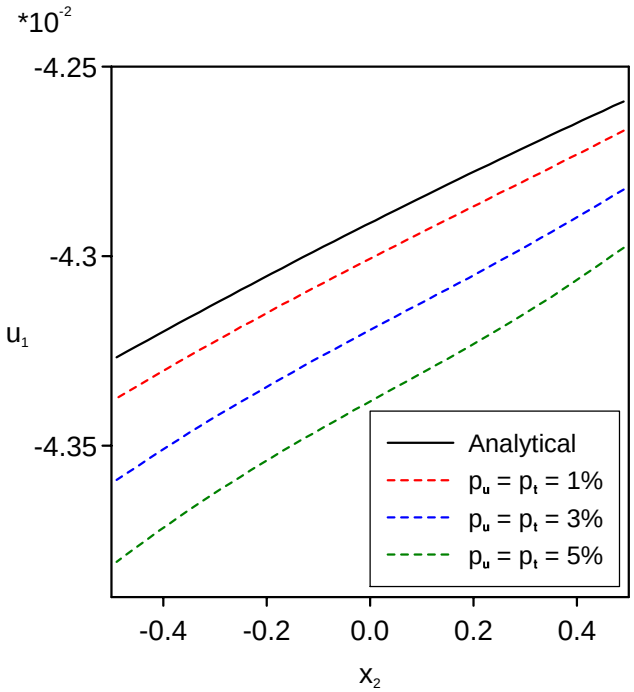

(c) Example 3: $u_1|_{\Gamma_2}$

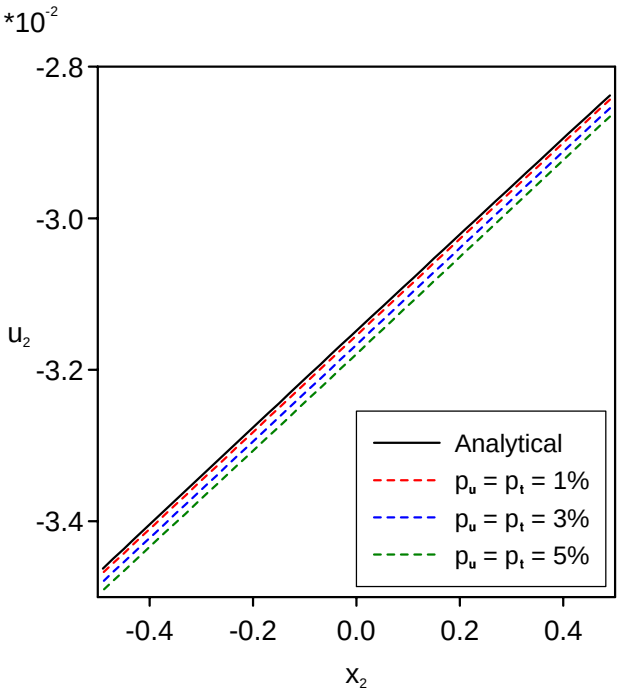

(d) Example 3: $u_2|_{\Gamma_2}$

Figure 14:

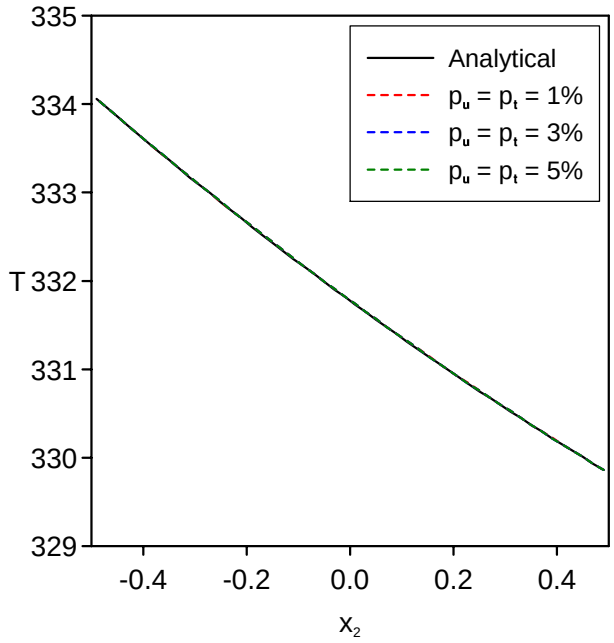

(a) Example 3: $T|_{\Gamma_2}$

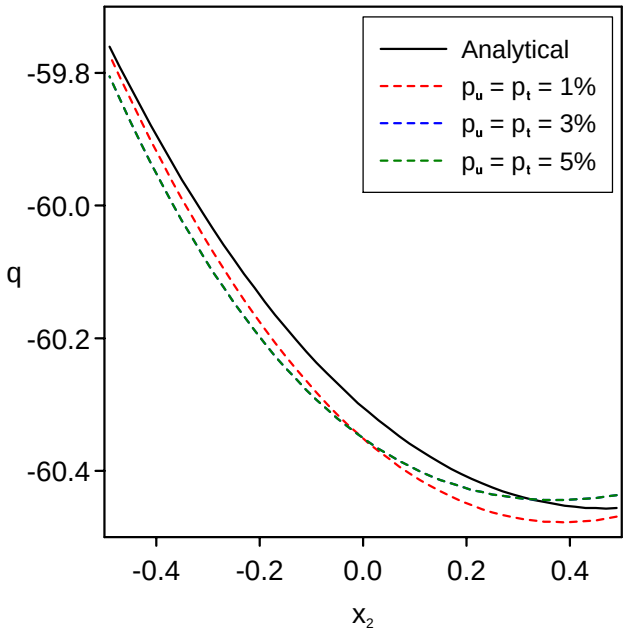

(b) Example 3: $q|_{\Gamma_2}$

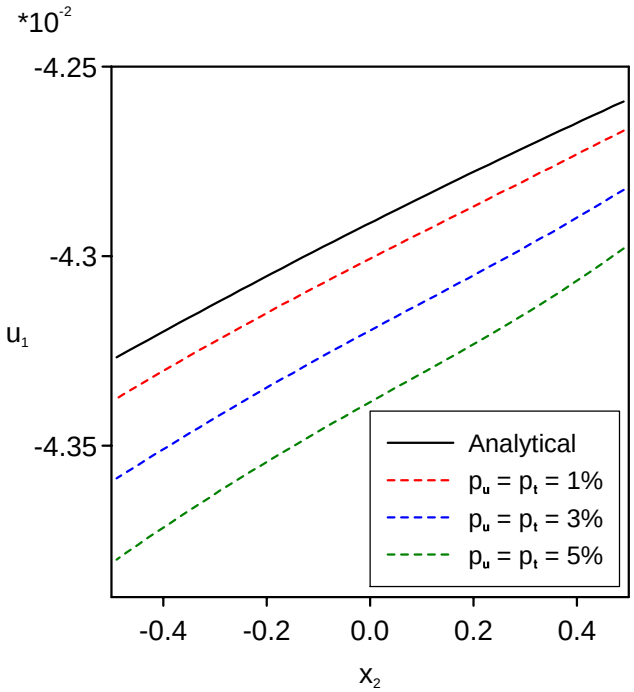

(c) Example 3: $u_1|_{\Gamma_2}$

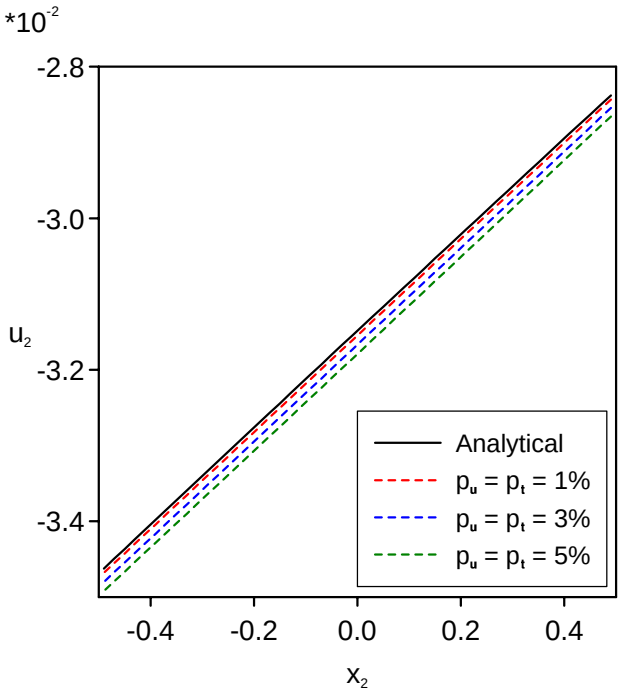

(d) Example 3: $u_2|_{\Gamma_2}$

Figure 15:

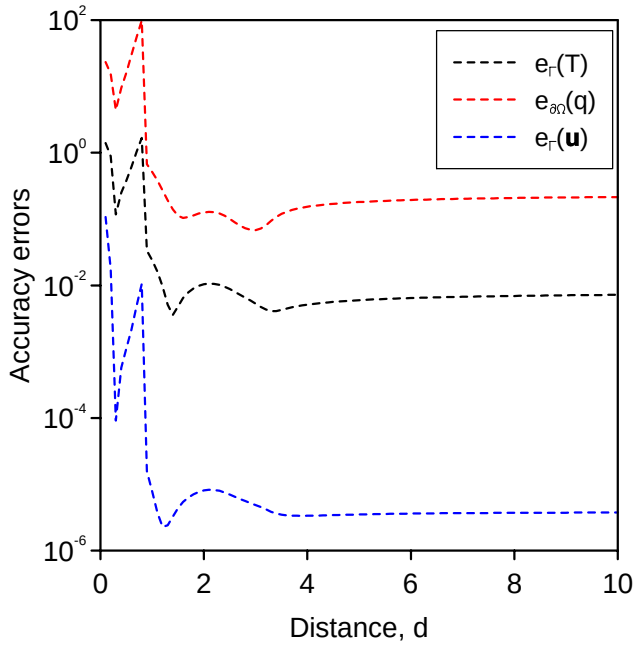

(a) Example 1: TRM–LC

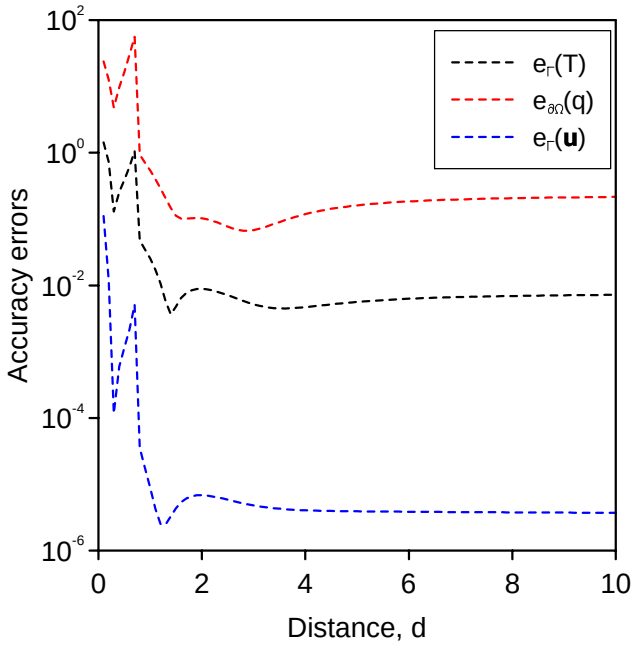

(b) Example 1: DSVD–LC

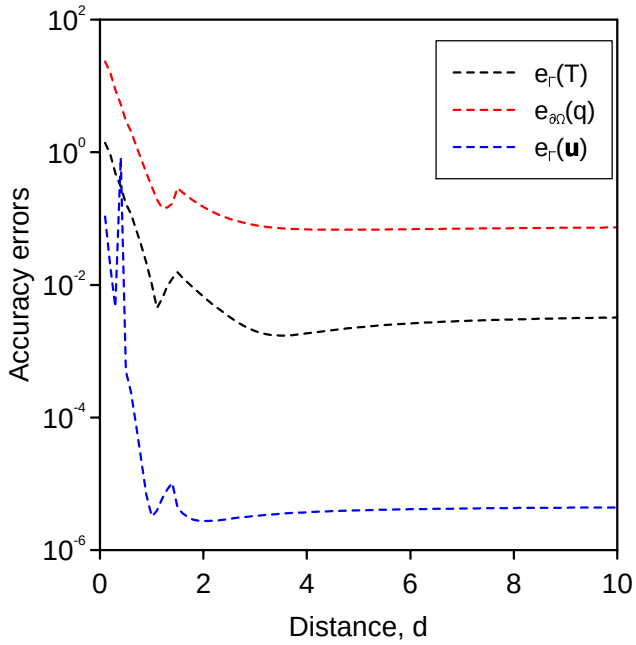

(c) Example 1: TSVD–DP

Figure 16:

Method	$p_T = p_{\mathbf{u}} = p_{\mathbf{t}}$	λ or k	$e_{\Gamma_2}(T)$	$e_{\partial\Omega}(q)$	$e_{\Gamma_2}(\mathbf{u})$
TRM–LC	1%	5.52×10^{-3}	1.04×10^{-2}	1.26×10^{-1}	8.06×10^{-6}
	3%	2.32×10^{-2}	6.92×10^{-3}	1.12×10^{-1}	1.96×10^{-5}
	5%	3.32×10^{-2}	1.02×10^{-2}	1.55×10^{-1}	4.73×10^{-5}
TRM–GCV	1%	4.35×10^{-14}	4.51×10^{1}	3.82×10^{3}	3.74×10^{0}
	3%	4.35×10^{-14}	1.35×10^{2}	1.15×10^{4}	3.37×10^{1}
	5%	4.35×10^{-14}	2.52×10^{2}	1.91×10^{4}	9.36×10^{1}
TRM–DP	1%	2.19×10^{-2}	7.08×10^{-3}	1.54×10^{-1}	3.38×10^{-6}
	3%	5.04×10^{-2}	1.29×10^{-2}	2.70×10^{-1}	7.35×10^{-5}
	5%	7.05×10^{-2}	1.60×10^{-2}	3.39×10^{-1}	2.35×10^{-4}
DSVD–LC	1%	6.55×10^{-3}	8.88×10^{-3}	1.03×10^{-1}	6.85×10^{-6}
	3%	2.10×10^{-2}	8.31×10^{-3}	1.01×10^{-1}	2.32×10^{-5}
	5%	3.62×10^{-2}	8.73×10^{-3}	1.66×10^{-1}	4.13×10^{-5}
DSVD–GCV	1%	1.14×10^{-14}	1.15×10^{2}	1.25×10^{4}	1.52×10^{1}
	3%	1.14×10^{-14}	3.46×10^{2}	3.74×10^{4}	1.37×10^{2}
	5%	1.14×10^{-14}	5.76×10^{2}	6.24×10^{4}	3.81×10^{2}
DSVD–DP	1%	4.11×10^{-3}	1.42×10^{-2}	3.18×10^{-1}	3.12×10^{-5}
	3%	1.12×10^{-2}	9.92×10^{-3}	3.05×10^{-1}	1.61×10^{-4}
	5%	1.85×10^{-2}	7.38×10^{-3}	2.89×10^{-1}	4.00×10^{-4}
TSVD–LC	1%	10	6.94×10^{-2}	1.21×10^{0}	6.41×10^{-3}
	3%	10	6.61×10^{-2}	1.21×10^{0}	5.79×10^{-3}
	5%	10	6.30×10^{-2}	1.21×10^{-1}	5.22×10^{-3}
TSVD–GCV	1%	110	5.86×10^{1}	5.45×10^{3}	5.41×10^{0}
	3%	110	1.76×10^{2}	1.63×10^{4}	4.87×10^{1}
	5%	110	2.93×10^{2}	2.72×10^{4}	1.35×10^{2}
TSVD–DP	1%	26	6.64×10^{-3}	1.50×10^{-1}	2.74×10^{-6}
	3%	17	1.71×10^{-3}	2.40×10^{-1}	3.31×10^{-5}
	5%	17	1.43×10^{-2}	2.59×10^{-1}	1.02×10^{-4}

Table 1: The values of the regularization parameter λ or the truncation number k, and the corresponding accuracy RMS errors, $e_{\Gamma_2}(T)$, $e_{\partial\Omega}(q)$ and $e_{\Gamma_2}(\mathbf{u})$, obtained using the regularization methods (R1)–(R3) with the criteria (C1)–(C3) for various amounts of noise in the data (11a)–(11c), i.e. $p_T = p_{\mathbf{u}} = p_{\mathbf{t}} \in \{1\%, 3\%, 5\%\}$, for the inverse problem (B) given by Example 1 with $\theta_0 = \pi$.

Method	θ_0	$p_T = p_{\mathbf{u}} = p_{\mathbf{t}}$	λ or k	$e_{\Gamma_2}(T)$	$e_{\partial\Omega}(q)$	$e_{\Gamma_2}(\mathbf{u})$
TRM–LC	$4\pi/3$	1%	7.93×10^{-3}	1.60×10^{-3}	4.08×10^{-2}	1.98×10^{-6}
		3%	2.83×10^{-2}	2.33×10^{-3}	1.37×10^{-1}	5.98×10^{-6}
		5%	4.22×10^{-2}	2.49×10^{-3}	1.83×10^{-1}	1.03×10^{-5}
	π	1%	5.52×10^{-3}	1.04×10^{-2}	1.26×10^{-1}	8.06×10^{-6}
		3%	2.32×10^{-2}	6.92×10^{-3}	1.12×10^{-1}	1.96×10^{-5}
		5%	3.32×10^{-2}	1.02×10^{-2}	1.55×10^{-1}	4.73×10^{-5}
	$2\pi/3$	1%	4.35×10^{-3}	6.62×10^{-3}	1.72×10^{-1}	4.24×10^{-6}
		3%	1.40×10^{-2}	1.04×10^{-2}	9.30×10^{-2}	4.42×10^{-5}
		5%	2.13×10^{-2}	1.18×10^{-2}	7.58×10^{-2}	1.04×10^{-4}
DSVD–LC	$4\pi/3$	1%	7.98×10^{-3}	1.58×10^{-3}	4.04×10^{-2}	1.97×10^{-6}
		3%	2.52×10^{-2}	1.59×10^{-3}	1.19×10^{-1}	8.21×10^{-6}
		5%	4.27×10^{-2}	2.54×10^{-3}	1.85×10^{-1}	9.73×10^{-6}
	π	1%	6.55×10^{-3}	8.88×10^{-3}	1.03×10^{-1}	6.85×10^{-6}
		3%	2.10×10^{-2}	8.31×10^{-3}	1.01×10^{-1}	2.32×10^{-5}
		5%	3.62×10^{-2}	8.73×10^{-3}	1.66×10^{-1}	4.13×10^{-5}
	$2\pi/3$	1%	5.49×10^{-3}	5.00×10^{-3}	1.30×10^{-1}	4.31×10^{-6}
		3%	1.81×10^{-2}	3.71×10^{-3}	7.47×10^{-2}	4.28×10^{-4}
		5%	3.25×10^{-2}	1.82×10^{-2}	3.00×10^{-1}	6.34×10^{-5}
TSVD–DP	$4\pi/3$	1%	25	3.09×10^{-3}	3.81×10^{-2}	2.60×10^{-6}
		3%	13	1.35×10^{-2}	3.27×10^{-1}	7.00×10^{-4}
		5%	13	1.07×10^{-2}	3.32×10^{-1}	5.57×10^{-4}
	π	1%	26	6.64×10^{-3}	1.50×10^{-1}	2.74×10^{-6}
		3%	17	1.71×10^{-3}	2.40×10^{-1}	3.31×10^{-5}
		5%	17	1.43×10^{-2}	2.59×10^{-1}	1.02×10^{-4}
	$2\pi/3$	1%	21	8.92×10^{-3}	1.26×10^{-1}	9.80×10^{-6}
		3%	21	2.94×10^{-2}	2.85×10^{-1}	9.52×10^{-5}
		5%	21	5.05×10^{-2}	4.71×10^{-1}	2.70×10^{-4}

Table 2: The values of the regularization parameter λ or the truncation number k, and the corresponding accuracy RMS errors, $e_{\Gamma_2}(T)$, $e_{\partial\Omega}(q)$ and $e_{\Gamma_2}(\mathbf{u})$, obtained using the regularization methods (R1)–(R3) with the best corresponding selection criteria (C1)–(C3) for various amounts of noise in the data (11a)–(11c), for the inverse problem (B) given by Example 1 with $\theta_0 \in \{4\pi/3, \pi, 2\pi/3\}$.

Method	$p_T = p_{\mathbf{u}}$	λ or k	$e_{\Gamma_2}(T)$	$e_{\Gamma_2}(q)$	$e_{\Gamma_2}(\mathbf{u})$	$e_{\Gamma_2}(\mathbf{t})$
TRM–LC	1%	2.84×10^{-3}	4.92×10^{-3}	1.14×10^{-2}	9.48×10^{-6}	7.90×10^{-5}
	3%	1.32×10^{-2}	7.65×10^{-3}	9.88×10^{-3}	2.24×10^{-4}	2.70×10^{-4}
	5%	1.97×10^{-2}	1.16×10^{-2}	1.22×10^{-2}	1.20×10^{-3}	1.23×10^{-3}
TRM–GCV	1%	1.69×10^{-2}	2.41×10^{-3}	2.71×10^{-3}	7.51×10^{-4}	7.53×10^{-4}
	3%	3.58×10^{-2}	6.17×10^{-3}	4.67×10^{-3}	9.85×10^{-3}	1.12×10^{-2}
	5%	6.15×10^{-2}	9.48×10^{-3}	5.13×10^{-3}	3.68×10^{-2}	4.23×10^{-2}
TRM–DP	1%	2.72×10^{-2}	2.19×10^{-3}	1.93×10^{-3}	4.31×10^{-3}	4.78×10^{-3}
	3%	6.37×10^{-2}	5.77×10^{-3}	3.06×10^{-3}	3.97×10^{-2}	4.57×10^{-2}
	5%	1.06×10^{-1}	9.17×10^{-3}	4.16×10^{-3}	7.82×10^{-2}	8.82×10^{-2}
DSVD–LC	1%	2.90×10^{-3}	4.90×10^{-3}	1.13×10^{-2}	9.34×10^{-6}	7.77×10^{-5}
	3%	9.12×10^{-3}	8.66×10^{-3}	1.40×10^{-2}	5.76×10^{-5}	1.89×10^{-4}
	5%	1.58×10^{-2}	1.22×10^{-2}	1.43×10^{-2}	4.38×10^{-4}	5.71×10^{-4}
DSVD–GCV	1%	2.52×10^{-3}	4.82×10^{-3}	1.25×10^{-2}	1.85×10^{-4}	2.51×10^{-4}
	3%	3.79×10^{-3}	1.26×10^{-2}	3.03×10^{-2}	3.94×10^{-4}	9.68×10^{-4}
	5%	6.10×10^{-3}	1.80×10^{-2}	3.92×10^{-2}	9.64×10^{-4}	1.71×10^{-3}
DSVD–DP	1%	2.52×10^{-3}	4.82×10^{-3}	1.25×10^{-2}	1.85×10^{-4}	2.51×10^{-4}
	3%	7.61×10^{-3}	1.02×10^{-2}	2.08×10^{-2}	1.58×10^{-3}	1.49×10^{-3}
	5%	1.16×10^{-2}	1.47×10^{-2}	2.69×10^{-2}	3.31×10^{-3}	3.05×10^{-3}
TSVD–LC	1%	82	5.79×10^{-3}	1.38×10^{-2}	1.49×10^{-5}	1.37×10^{-4}
	3%	150	3.05×10^{-1}	1.88×10^{0}	1.39×10^{-2}	1.89×10^{0}
	5%	150	5.08×10^{-1}	3.13×10^{0}	3.86×10^{-2}	5.25×10^{0}
TSVD–GCV	1%	40	1.89×10^{-3}	8.73×10^{-4}	6.61×10^{-6}	2.78×10^{-5}
	3%	40	5.66×10^{-3}	2.62×10^{-3}	3.05×10^{-5}	6.35×10^{-5}
	5%	7	4.75×10^{-3}	5.51×10^{-7}	1.29×10^{-1}	1.55×10^{-1}
TSVD–DP	1%	40	1.89×10^{-3}	8.73×10^{-4}	6.61×10^{-6}	2.78×10^{-5}
	3%	40	5.66×10^{-3}	2.62×10^{-3}	3.05×10^{-5}	6.35×10^{-5}
	5%	40	9.44×10^{-3}	4.37×10^{-3}	7.24×10^{-5}	1.14×10^{-4}

Table 3: The values of the regularization parameter λ or the truncation number k, and the corresponding accuracy RMS errors, $e_{\Gamma_2}(T)$, $e_{\Gamma_2}(q)$, $e_{\Gamma_2}(\mathbf{u})$ and $e_{\Gamma_2}(\mathbf{t})$, obtained using the regularization methods (R1)–(R3) with the criteria (C1)–(C3) for various amounts of noise in the data (10a)–(10b), for the inverse problem (A) given by Example 2.

Method	$p_{\mathbf{u}} = p_{\mathbf{t}}$	λ or k	$e_{\Gamma_2}(T)$	$e_{\partial\Omega}(q)$	$e_{\Gamma_2}(\mathbf{u})$
TRM–LC	1%	8.08×10^{-7}	4.69×10^{-6}	5.30×10^{-4}	1.22×10^{-6}
	3%	1.87×10^{-6}	3.78×10^{-6}	4.27×10^{-4}	1.10×10^{-5}
	5%	3.64×10^{-6}	2.43×10^{-6}	2.73×10^{-4}	3.06×10^{-5}
TRM–GCV	1%	1.39×10^{-5}	3.66×10^{-7}	7.02×10^{-5}	1.22×10^{-6}
	3%	2.71×10^{-5}	1.20×10^{-6}	2.00×10^{-4}	1.10×10^{-5}
	5%	3.78×10^{-5}	4.41×10^{-6}	5.67×10^{-4}	3.06×10^{-5}
TRM–DP	1%	2.78×10^{-5}	1.36×10^{-6}	2.17×10^{-4}	1.22×10^{-6}
	3%	5.42×10^{-5}	1.12×10^{-5}	1.37×10^{-3}	1.10×10^{-5}
	5%	7.58×10^{-5}	2.13×10^{-5}	2.58×10^{-3}	3.07×10^{-5}
DSVD–LC	1%	5.79×10^{-7}	4.26×10^{-6}	4.82×10^{-4}	1.22×10^{-6}
	3%	1.87×10^{-6}	3.78×10^{-6}	4.27×10^{-4}	1.10×10^{-5}
	5%	3.08×10^{-6}	2.76×10^{-6}	3.10×10^{-4}	3.06×10^{-5}
DSVD–GCV	1%	2.51×10^{-7}	8.31×10^{-5}	9.27×10^{-3}	1.23×10^{-6}
	3%	6.84×10^{-7}	9.02×10^{-5}	1.01×10^{-2}	1.10×10^{-5}
	5%	1.13×10^{-6}	9.06×10^{-5}	1.01×10^{-2}	3.06×10^{-5}
DSVD–DP	1%	5.97×10^{-7}	3.31×10^{-5}	3.71×10^{-3}	1.23×10^{-6}
	3%	1.91×10^{-6}	2.92×10^{-5}	3.33×10^{-3}	1.10×10^{-5}
	5%	3.16×10^{-6}	2.88×10^{-5}	3.34×10^{-3}	3.06×10^{-5}
TSVD–LC	1%	8	1.93×10^{-2}	1.18×10^{0}	2.25×10^{-4}
	3%	8	1.93×10^{-2}	1.18×10^{0}	1.64×10^{-4}
	5%	8	1.93×10^{-2}	1.18×10^{0}	1.15×10^{-4}
TSVD–GCV	1%	42	4.38×10^{-6}	5.15×10^{-4}	1.22×10^{-6}
	3%	37	4.62×10^{-6}	6.20×10^{-4}	1.11×10^{-5}
	5%	37	4.62×10^{-6}	6.20×10^{-4}	3.08×10^{-5}
TSVD–DP	1%	426	4.38×10^{-6}	5.15×10^{-4}	1.22×10^{-6}
	3%	376	4.62×10^{-6}	6.20×10^{-4}	1.11×10^{-5}
	5%	376	4.62×10^{-6}	6.20×10^{-4}	3.08×10^{-5}

Table 4: The values of the regularization parameter λ or the truncation number k, and the corresponding accuracy RMS errors, $e_{\Gamma_2}(T)$, $e_{\partial\Omega}(q)$ and $e_{\Gamma_2}(\mathbf{u})$, obtained using the regularization methods (R1)–(R3) with the criteria (C1)–(C3) for various amounts of noise in the data (11a)–(11c), for the inverse problem (B) given by Example 3.